國立交通大學

電機學院光電顯示科技產業研發碩士班

碩士論文

應用人眼視覺特性之低功耗液晶顯示技術

Minimizing LCD Power Consumption by Using Temporal Properties of Vision System

研究生：許枝福

指導教授：鄭惟中 博士

中華民國九十六年二月

應用人眼視覺特性之低功耗液晶顯示技術

Minimizing LCD Power Consumption by Using Temporal Properties of Vision System

研 究 生: 許枝福　　Student: Chih-Fu Hsu

指導教授: 鄭惟中 博士　　Advisor: Dr. Wei-Chung Cheng

國立交通大學

電機學院光電顯示科技產業研發碩士班

碩士論文

A Thesis

Submitted to College of Electrical and Computer Engineering

National Chiao Tung University

in Partial Fulfillment of the Requirements

for the Degree of Master

in

Industrial Technology R & D Master Program on

Photonics and Display Technologies

February 2007

Hsinchu, Taiwan, Republic of China

中華民國九十六年二月

應用人眼視覺特性之低功耗液晶顯示技術

碩士研究生：許枝福　　指導教授：鄭惟中 博士

國立交通大學 電機學院

中文摘要

液晶顯示器由於其輕薄之特性，已大量被應用在可攜式產品中，但由於電池容量與尺寸限制，可攜式產品一般都不能長時間的連續使用；在近幾年研究中得知，液晶顯示器的背光模組所消耗能量將近整體系統的五成；為了延長電池的使用時間，如何降低背光模組的耗電變成重要的課題。我們研究的目標是利用人眼視覺的視頻特性—感知亮度增強效應(Brücke effect)，提出新的背光源驅動技術，透過調整背光強度、閃爍頻率及發光週期，來降低背光源的功率消耗並保持在液晶顯示器上所感受的亮度。實驗結果顯示，在相同的感知亮度及有限的畫面閃爍下，可以降低背光模組之功率消耗。

Minimizing LCD Power Consumption by Using Temporal Properties of Vision System

Student: Chih-Fu Hsu Advisor: Dr. Wei-Chung Cheng

National Chiao Tung University

ABSTRACT

This paper presents a novel backlight driving technique for liquid crystal displays. By scaling the intensity, frequency, and duty cycle of the backlight, this technique not only increases the perceived brightness but also saves the power. The increased brightness comes from a perceptual effect of temporal vision – a brief flash appears brighter than a steady light of the same intensity, called Brücke brightness enhancement effect. Due to the experimental data, the backlight power consumption decreases at the cost of flickering. We performed visual experiments to parameterize the Brücke effect and derived an optimization algorithm accordingly. To demonstrate the potential power savings of this technique, we profiled the power consumption of an Apple iPod and fabricated an LED driving module.

致　　謝

回顧過去七百多個日子，每一分每一秒都是感動，也讓我的人生旅途上增添了繽紛色彩。很高興能在交通大學完成我第一個碩士學位，在此，謹以此論文來對曾經陪伴我度過重重考驗的諸位，表達我最誠摯的謝意。

首先，由衷感謝指導教授鄭惟中老師，因為有您的循循善誘，敦促我朝正確的研究方向前進，並時常給予機會讓我去嘗試及挑戰，更在我受挫時給於鼓勵與支持，謝謝您的栽培與鍛鍊，我才會有今日之成就。此外，感謝口試委員許根玉教授、戴亞翔副教授、戴文智博士的細心指導，使本文得以更加完善。

在求學的日子裡，首先要感謝實驗室夥伴建智、健富、愷均以及志男，因為有您們攜手相伴，讓我得以勇往直前。另外，還要感謝動物家族俞文、映頻、佳峰、子怡和永志以及其它親愛的同學們，因為有您的陪伴，讓這兩年研究生的生活更多姿多采。我也要特別感謝所辦小姐美貞、琬姝、歆怡等人協助，與你們共事真的很愉快。

另外，還要感謝貴嵐以及Miss Chen，於春節期間協助校訂論文，占用您不少時間及精神，萬分感謝。

最後，要獻給敬愛的爸媽、摯愛虹伶及家人們，感謝你們的栽培、支持與鼓勵，讓我能夠全心全意去作研究，並順利完成此論文並取得碩士學位，這份喜悅與榮耀是屬於你們的。

許枝福　謹識於新竹
中華民國九十六年三月

Table of Contents

Figure Caption

List of Tables

Chapter 1

Introduction

1.1 Low Power Consumption in Portable Devices

The power consumption has been the critical issue for most battery-powered electronics. In literature, researchers have found that the display consumes a major portion of the total power consumption in portable devices. In Cheng's works, they have shown the TFT LCD backlight consumed almost half of the energy without any power management for the backlight module [Cheng 2004]. Although the hard disk drive consumes up to 54% of power, it consumes only 10% of total energy in the right of pie charts because the hard disk is not always running.

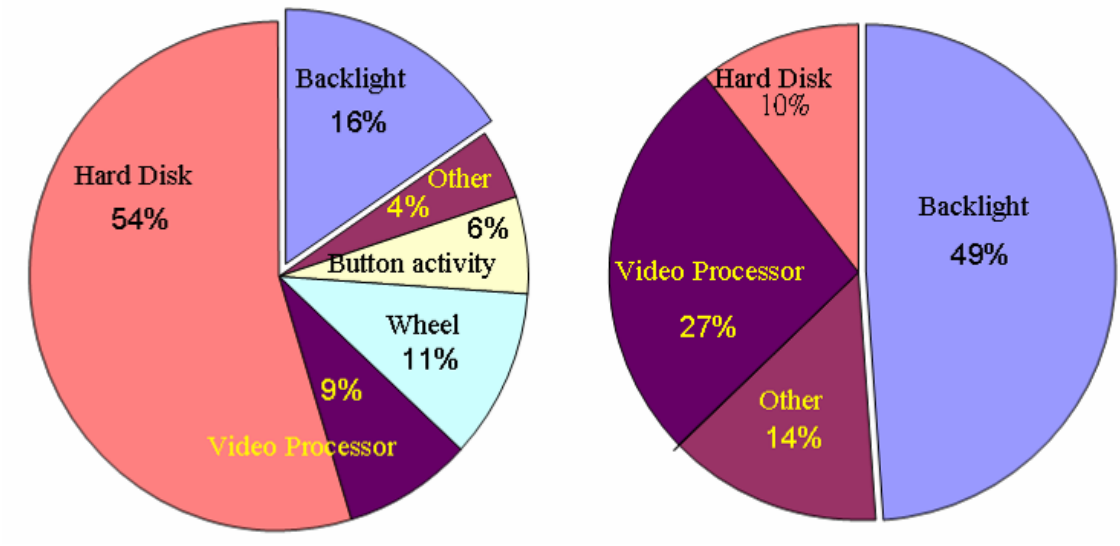

Figure 1-1: Power (left) and energy (right) breakdown of iPod playing a 323-second video clip. The backlight consumes 49% of total energy.

1.2 Optical Efficiency of TFT LCDs

The low optical efficiency is the major cause of the high power consumption of TFT LCD panel. The TFT LCD panel has low light efficiency because of its structure as shown in Figure 1-2. It consists of two major components -- TFT LCDs panel and backlight module. Each pixel on the panel can be considered as a light modulator, which depends on the value of each pixel of the source image to modulate the intensity of light. The TFT LCDs panel transmits light for a bright pixel and blocks light for a dark pixel. In other words, the image is formed by absorbing the light of dark pixel in a transmissive display. Therefore, different images, even dark ones, consume almost the same power. Briefly, only less than 5% of light can be delivered to the user, while the rest 95% is wasted in the structure of TFT LCDs as in Figure 1-2.

Generally three color filters -- red, green, and blue -- are used to display all colors. If we assume that the optical energy is evenly distributed in these three spectral regimes, then each color filter can transmit only one-third of the total optical energy. In other words, two-thirds of the energy is absorbed by the color filters. In common display design, the transmission bandwidth of the color filter is usually very wide to allow a higher brightness at the expense of lower color purity. In order to enhance color saturation, the color filters have a narrowed bell-shape spectral transmission curve centered at their respective colors that match the peaks of the RGB-enhanced backlights. Thus the color filters can only transmit less than one-third of the total energy. This explains the typical transmission of only 20% as shown in Table 1-1.

Table 1-1: Transmission of Various LCD Components [YEH 1999]

Layer	Transmission
Polarizer	43%
Color filter	25%
TFT aperture ratio	80%

Liquid Crystal	95%
Analyzer	80%
Overall (color LCDs)	5%

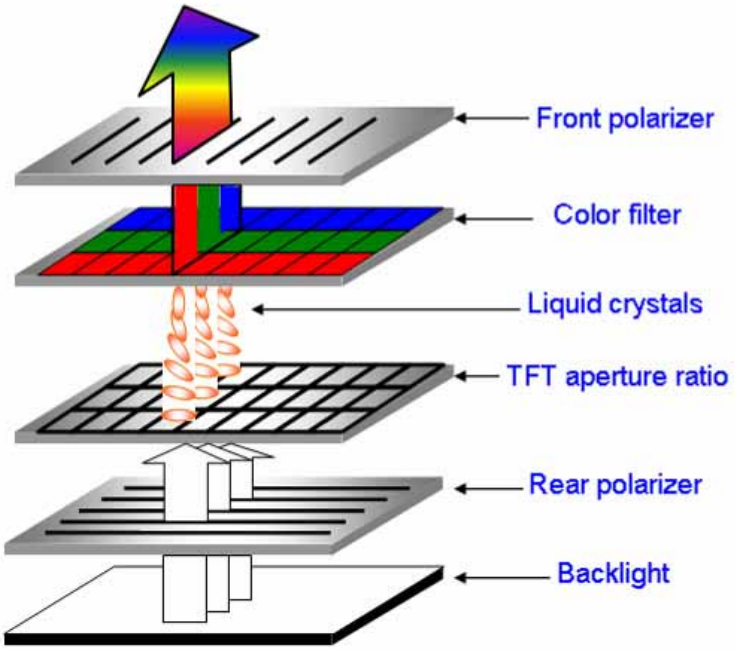

Figure 1-2: The structure of a TFT LCD consists of six layers from top to bottom: front polarizer, color filter, LC, TFT, rear polarizer, and backlight module.

More than 50% of light is blocked by the rear polarizer. The *aperture ratio*, representing the percentage of the area not occupied by the TFT LCDs and wires, depends on the pixel circuit design and can be as high as 95%. About 5% of light is absorbed by the liquid crystals. Each of the red, green, and blue color filters transmits roughly one-third of visible wavelength. The front polarizer blocks another 10% right before the light exits the panel. The power consumption of the LCD panel is almost constant so it is independent of the panel transmittance. On the contrary, the power consumption of the backlight is a strong function of its output luminance.

1.3 Objective

The main objective of this thesis is to propose a novel backlight driving technique for

low-power liquid crystal displays. By scaling the intensity, frequency, and duty cycle of the backlight, this technique not only increases the perceived brightness but also prolongs the service time of rechargeable batteries. A great amount of energy can be saved at the cost of flickering.

1.4 Organization

The thesis is organized as follows: the previous works of the temporal vision phenomena are presented in Chapter 2. In Chapter 3, the considerations of the fabrication of RGB LED backlit LCDs as well as the major measurement equipment used for characterization are described. In Chapter 4, the principles including backlight scaling, blinking backlight, and light enhancement of LED backlight LCDs will be presented. In Chapter 5, the experimental results including psychophysical experiments are demonstrated. In Chapter 6, the summary of the dissertation and the future works are given.

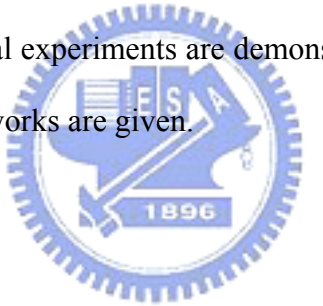

Chapter 2

Literature Review

The most primitive works with respect to temporal vision and contrast sensitivity functions are reviewed in this chapter. Related researches, such as backlight enhancement, critical fusion flicker frequency (CFFF), and temporal contrast sensitivity function (TCSF), will be introduced. More detail about CSF like achromatic contrast sensitivity function, spatial-temporal contrast sensitivity surface, and chromatic contrast sensitivity function will be introduced in the end of this chapter.

2.1 Brightness Enhancement of Flashing Light

Three fundamental phenomena in temporal human vision are related to our study. The first is *Broca-Sulzer effect*, which states that the supra-threshold stimuli, whose duration is on the order of 50-100 milliseconds, appear brighter than stimuli of either shorter or longer durations [Broca 1902].

The second, *Brücke-Bartley effect,* is that when a light is flickered on and off, its brightness varies according to the frequency of flicker, reaching a maximum over a narrow range of frequencies at approximately 5 to 20 Hz, depending on the intensity of the flickering light. The expression of the Brücke-Bartley effect was described in the middle row of Figure 2-2 [Moses 1987].

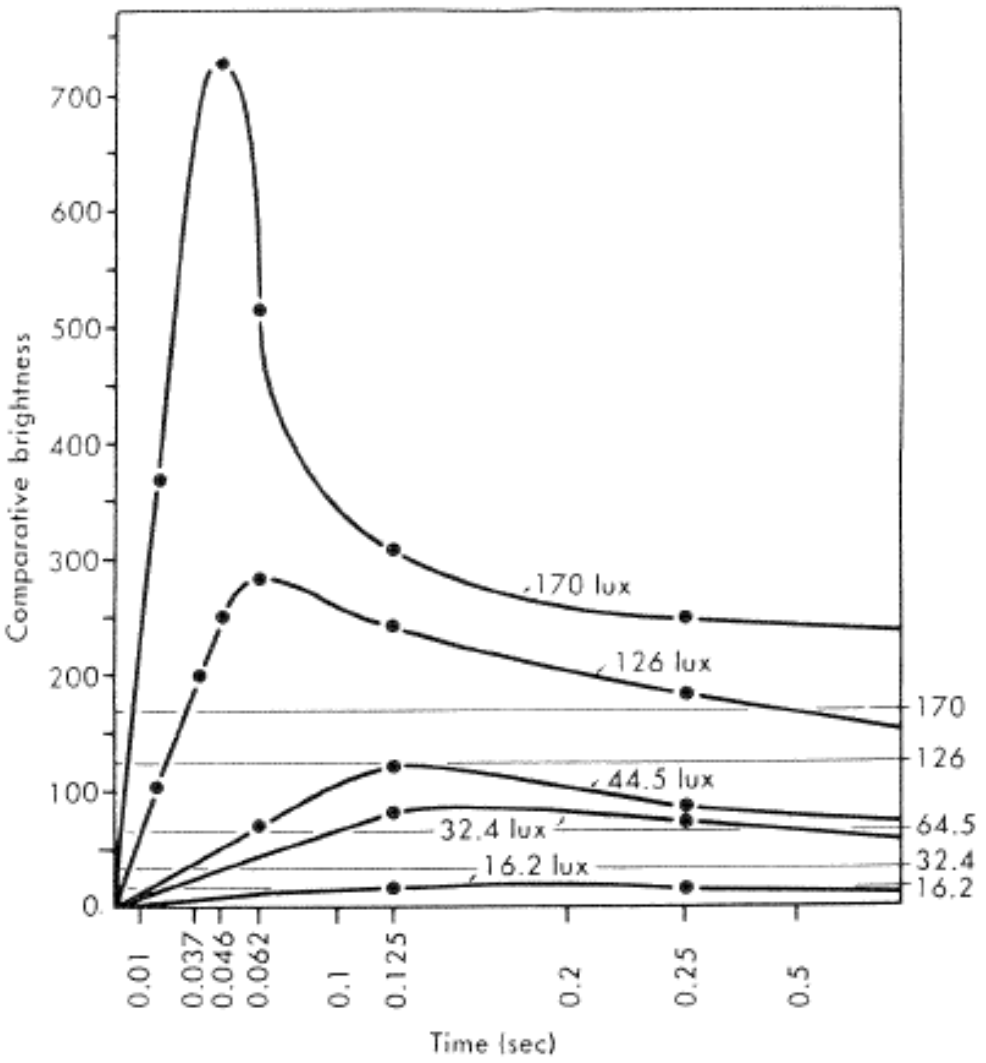

Figure 2-1: Broca-Sulzer effect: Brightness of flashes having various luminances, as functions of flash duration [Broca 1902]. For relatively bright stimuli, a transient peak of brightness occurs before the plateau is reached. This effect can produce the seeming paradox of a short flash appearing brighter than a longer flash of the same luminance.

The third, *Talbot-Plateau law,* states that the brightness of a temporally modulated stimulus, when fused, is equal to the brightness of a steady light with the same time-averaged luminance. The expression of the Talbot-Plateau law was described in the last row of Figure 2-2 given that the frequency exceeds the critical fusion frequency.

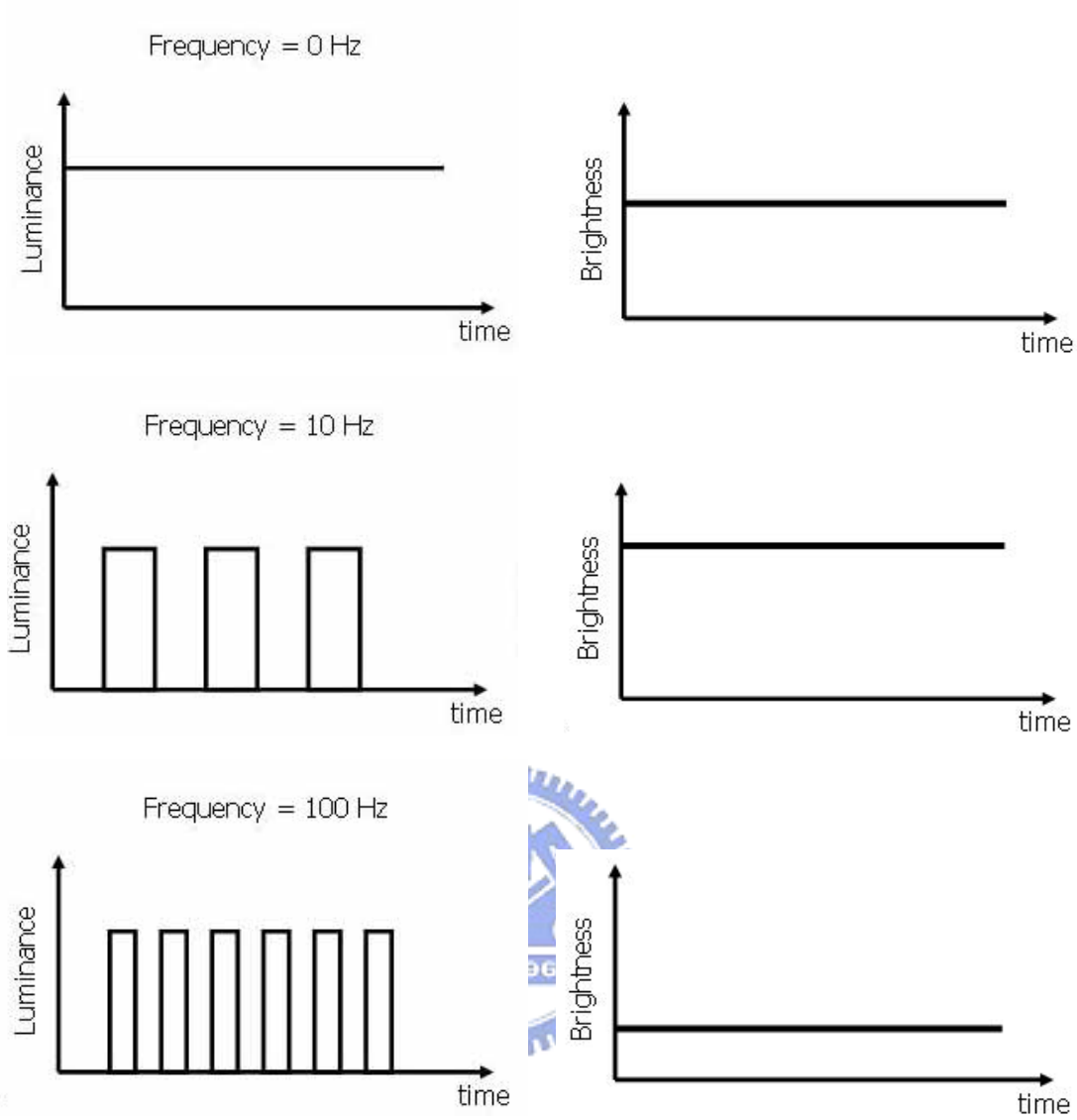

Figure 2-2: Comparison of the frequency and perceived brightness. The brightness at modulating frequency = 10 Hz is higher than the brightness at 0 Hz but the flicker can be seen. The brightness at modulating frequency = 100 Hz is similar but under the brightness at 0 Hz without flicker.

2.2 Critical Flicker Fusion Frequency

The critical flicker fusion frequency (CFFF), also called critical flicker frequency (CFF), indicates the transition from the perception of flicker to that of fusion, which occurs over a range of temporal frequencies. The *Ferry-Porter law* predicts that the CFFF increases as the luminance of the flashing stimulus increases. The CFFF is not only a function of luminance,

but also the stimulus size (by *Franit-Harper law*) and wavelength (by *Hecht-Shlaer law)*.

In 1987, Farrell proposed an analytical method for predicting whether a video display terminal will appear to flicker given the screen phosphor persistence, refresh frequencies, and other environmental factors such as ambient light level, the distance between the viewer and the display, etc. From the method, one can predict the maximum screen luminance and the minimum refresh frequency that result in a flicker-free display for a theoretical standard observer [Farrell 1987].

The CFFF is shown as a function of retinal illuminance describe in Figure 2-3.

$$f_{CFFF}(L) = a \cdot \log(L) + b \qquad (1)$$

where *a,* and *b* are coefficients and *L* is the retinal illuminance is also trolands in the equation (1).

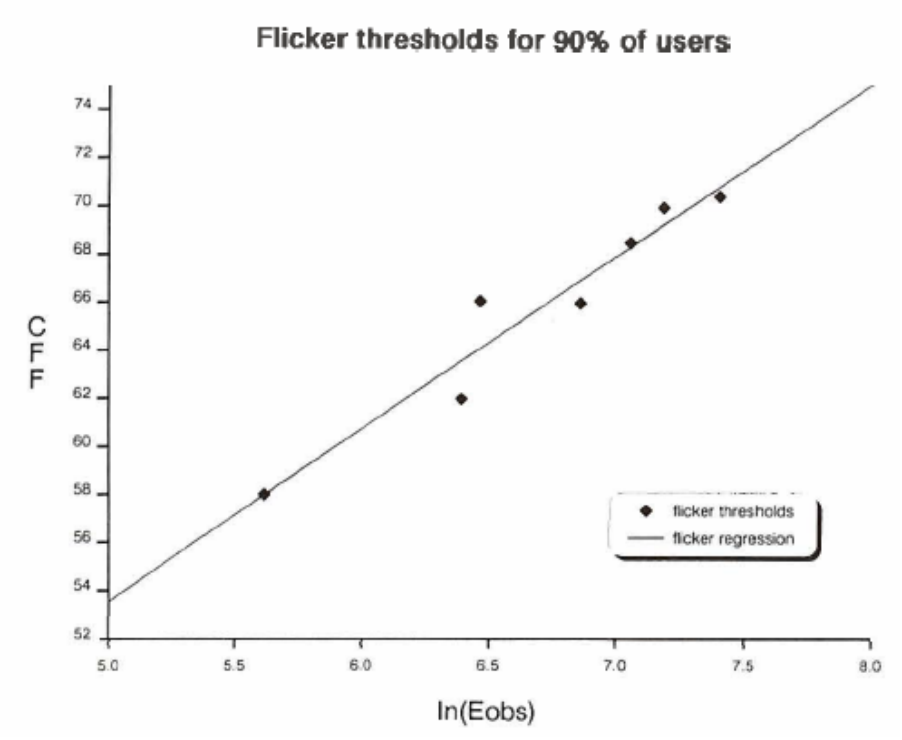

Figure 2-3: Critical flicker frequency in Hz estimated 90% of the user population plotted as a function of the natural logarithm of the absolute amplitude of the fundamental temporal frequency specified in units of retinal illuminance (trolands) [Farrell 1987].

2.3 Temporal Contrast Sensitivity Function

The spatial and temporal characteristics of human visual system are typically explored through measurement of contrast sensitivity functions. Contrast sensitivity functions in vision science are analogous to modulation transfer functions in imaging science. A contrast sensitivity function is defined by the threshold response to contrast (sensitivity is the inverse of threshold) as a function of spatial or temporal frequency. Visual stimuli varying sinusoidally in radiance as a function of time were introduced by Ives in 1922 [Kelly 1961]. The stimulus as a function of time has the form as below:

$$f(t) = B\,(\,1 + m\cos(wt)\,) \qquad (2)$$

Where m is relative amplitude (dimensionless), mB is absolute amplitude, B is adaptation level (average luminance), $2mB$ is flicker beam, and $(1\text{-}m)B$ is adaptation beam. The sinusoidal stimulus is illustrated as Figure 2-4. The relative amplitude or modulation ratio m is a measure of the successive contrast of the stimulus waveform, and hence is closely related to contrast measurements in general.

$$m = (\,f_{max} - f_{min}\,) / (\,f_{max} + f_{min}\,) \qquad (3)$$

In fact, the relative amplitude is the temporal analogue of the well-known *Michelson contrast* of interference fringes.

In the spatial domain, spatial vision can be characterized by the contrast sensitivity function CSF. A temporal contrast sensitivity function is a plot of how flicker varies with contrast and vice versa. Above the curve represents no flicker while flicker can be detected below the curve. The eye appears to be most sensitive to frequencies between 15 and 20 Hz at high luminances. At high luminances levels, less than 1% contrast is required to detect the stimuli and the high temporal frequency cut off is close to 60 Hz. At low light levels the maximum contrast is about 20% and the high temporal frequency cut off is approximately 15

Hz. To detect flicker at higher frequencies, higher contrast is required. The temporal resolution is not as efficient as at low luminances.

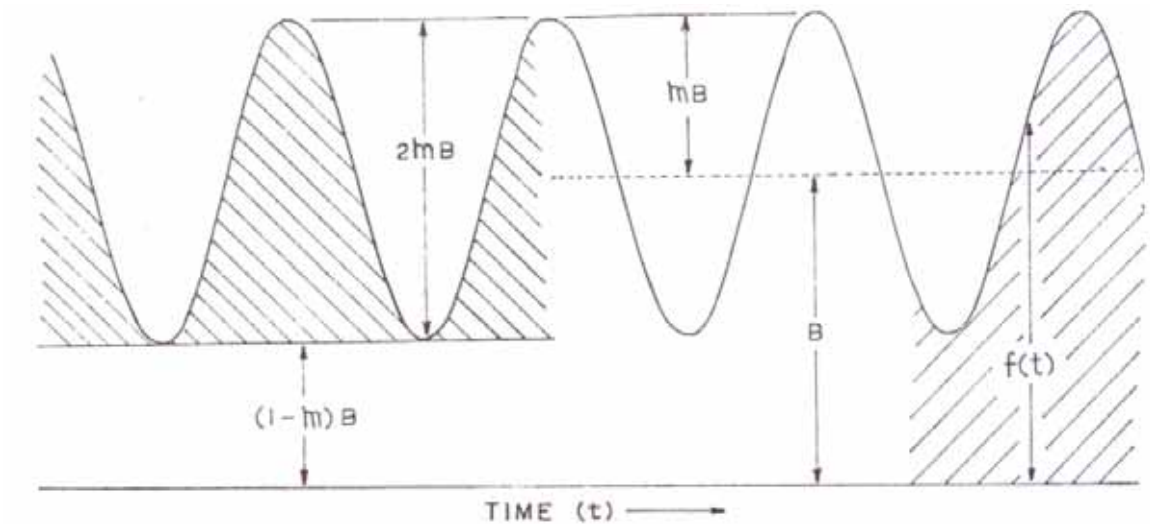

Figure 2-4: Sinusoidal stimulus waveform [Kelly 1961]. Where *m* is relative amplitude (dimensionless), *mB* is absolute amplitude, *B* is adaptation level (average luminance), *2mB* is flicker beam, and *(1-m)B* is adaptation beam.

Temporal vision deals with the way the visual system perceives changes in luminance as a function of time and is characterized by the temporal modulation transfer function. Figure 2-5 illustrates the amplitude of modulation in left column and the frequencies variation in bottom row. According to Figure 2-5 (top right), the human eye can not distinguish the very small luminance variation so that area beyond the curve is the fusion area, where the human eye perceives the amplitude modulated light as steady light. Higher sensitivity means the human eye can distinguish the small luminance difference. The critical fusion frequency is the frequency point cross the maximum amplitude modulation. It means that the human eye can not sense the luminance difference in axis of time.

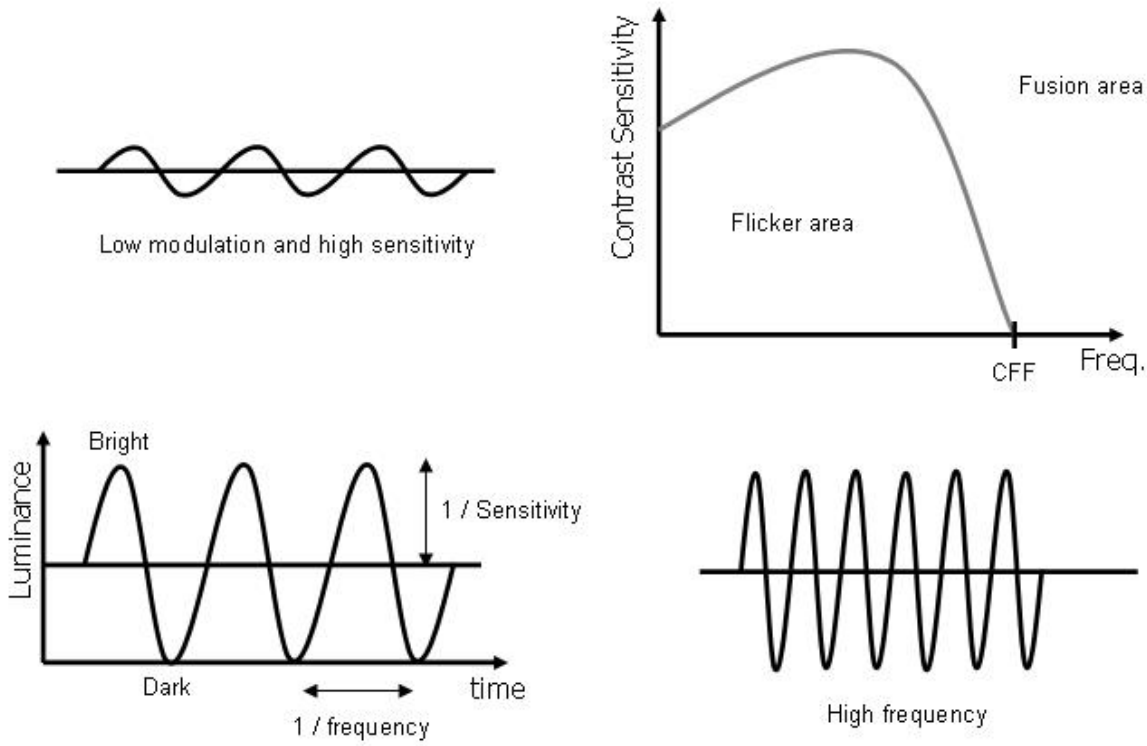

Figure 2-5: The modulation and the frequency of the sinusoidal stimulus in CSF. The left column described the modulation of the sinusoidal function, and top one had lower amplitude of modulation than the bottom one. The bottom row described the frequencies variation, and left one had lower frequency than the right one.

2.4 Achromatic Contrast Sensitivity Function

In the middle period of twentieth century, de Lange carried out an elaborate series of small-field, amplitude sensitivity measurements [de Lange 1957]. The human visual system is viewed as a black box, and its properties can be characterized by analyzing the way in which the visual stimuli are altered to produce visual sensation. De Lange's approach to the visual system was to attempt to determine the attenuation characteristics of the visual system as if it were a linear filter. He used a range of frequencies of sinusoidally changing light stimuli, while measuring the subjective perception of flicker. The perceived quantity was not physical but only detectable in the psychophysical behavior of human observers.

After de Lange's work, Kelly introduced an amplitude sensitivity measurement with

sinusoidal modulation stimulus, the amplitude thresholds are measured instead of the repetition rate thresholds usually obtained in flicker-fusion experiments. The observer's adaptation level can be held constant while his amplitude sensitivity is measured as a function of the modulation frequency [Kelly 1961].

Figure 2-4 exhibits modulation ratios *m* increasing downward correspond to just detectable flicker at each of frequencies tested. As described in Figure 2-6, Kelly's work has demonstrated that flicker perception is dependent on the relation between CFFF and the modulation sensitivity (m^{-1}). The quantity *m* is called the *modulation threshold* and used for a response criterion for the sensitivity of visual system. Such classic relationships as the *Ferry-Porter*, *Talbot-Plateu*, and *Weber-Fechner laws* can be derived from the present results.

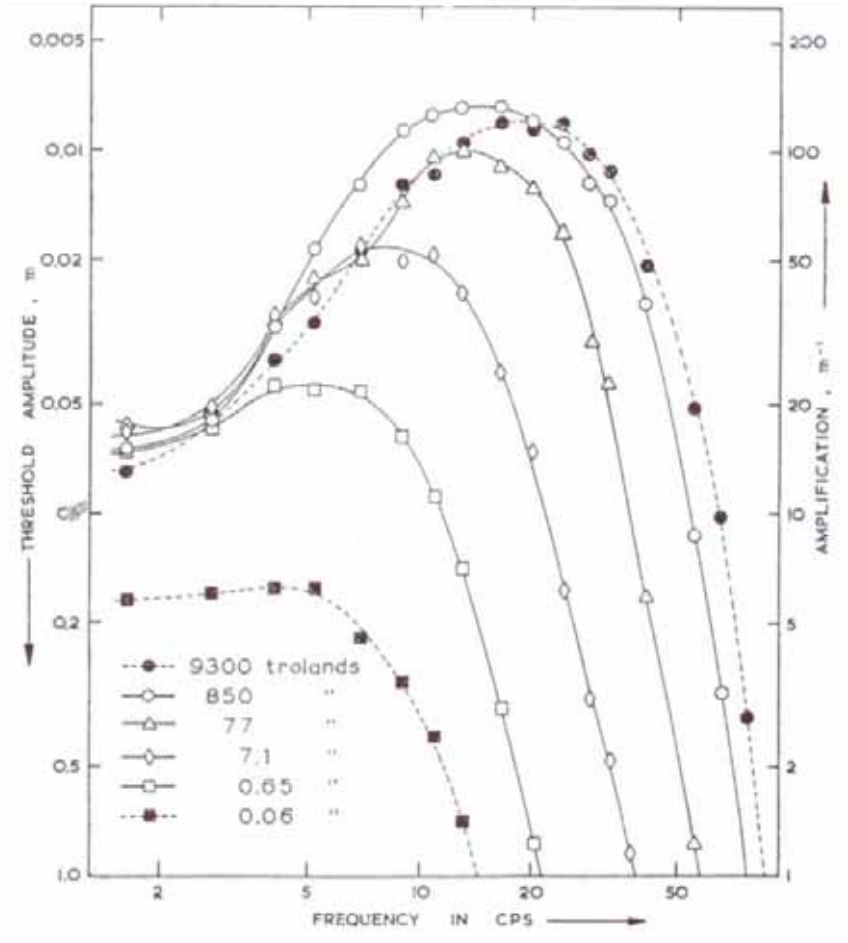

Figure 2-6: Temporal sensitivity function [Kelly 1961]. The amplitude sensitivity first rises to a maximum then falls off sharply for each curve with different illumination level on eyes.

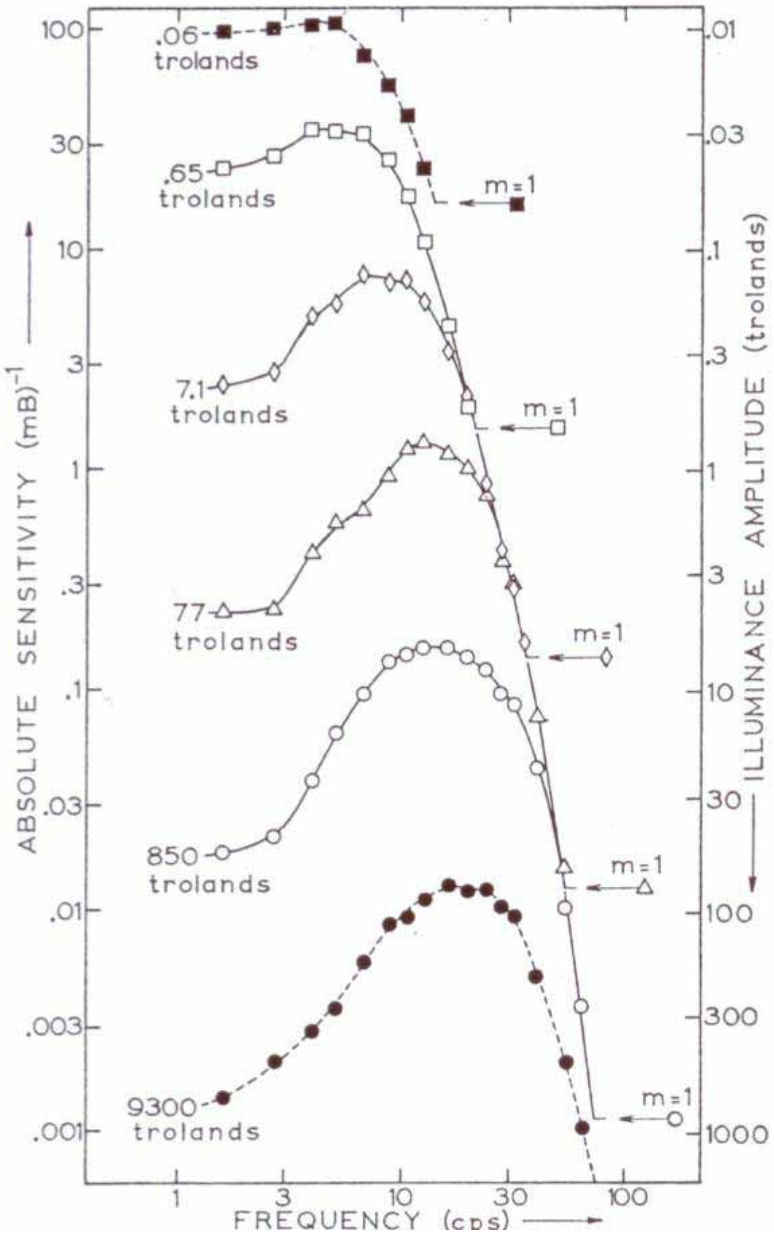

Figure 2-7: Absolute sensitivity function [Kelly 1961]. In absolute units, the amplitude sensitivity is greatest at the lowest adaptation level.

The Figure 2-7 shows absolute units. The amplitude sensitivity is the greatest at the lowest adaptation level. A common asymptote at high frequencies, the high-frequency threshold depends solely on the absolute amplitude *mB;* it does not matter whether a given amplitude is obtained by varying the adaptation level *B* or the modulation ratio *m*.

2.5 Spatial-temporal Contrast Sensitivity Surface

In the same decade, Kelly included the spatial frequency and drew a perspective view of three-dimensional spatio-temporal threshold surface [Kelly 1966]. Till 1971, Kelly addressed the spatio-temporal amplitude threshold surface again, with adaptation effects. The stimulus combined spatio-temporal sine-wave, the form as below:

$$\Phi(x,t) = B + \Delta B \cos(\alpha x) \cos(\omega t) \tag{4}$$

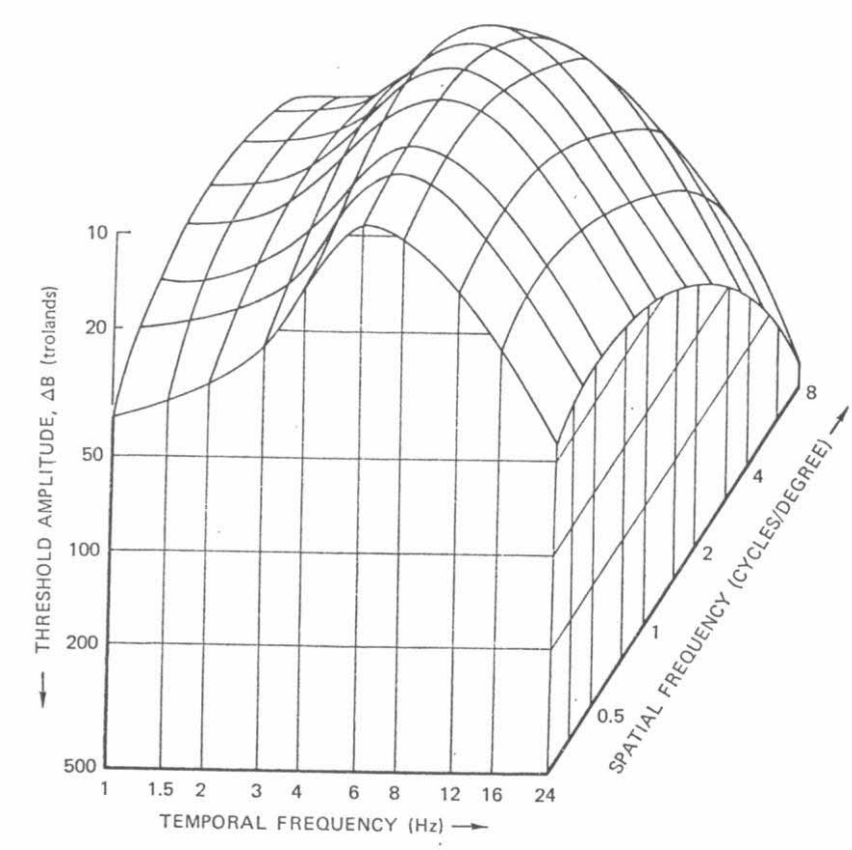

Figure 2-8: Spatio-temporal amplitude threshold surface [Kelly 1971]. It shown the threshold is a function of both temporal and spatial frequency.

Where $\alpha/2\pi$ is spatial frequency and $\omega/2\pi$ is temporal frequency, the spatio-temporal amplitude threshold ΔB as shown in Figure 2-8. Here we will consider how the shape of this surface varies with the adaptation level B. The adjacent bars of such a grating flicker in opposite phases, so that it was spatial average at any instant, and its temporal average at any point, are both constant and equal to B. Because ΔB cannot exceed B, the threshold is

frequently expressed in terms of normalized quantity $\Delta B/B$ usually is called the modulation. For any fixed value of B, spatio-temporal sine-wave thresholds can be plotted as a surface in a three-dimensional space, in which temporal and spatial frequencies are the independent variables. There is a rather flat maximum of sensitivity in the region of 5 to 15Hz and 2 to 6 cycles per degree; sensitivity decreases at higher and lower frequencies [Kelly 1971].

Before Kelly's report, Robson had measured the spatio-temporal sensitivity and give an equation as below:

$$F(x,t) = L(1 + m\ cos(2\pi f_S x)\ cos(2\pi f_T t))) \quad (5)$$

Where m is the contrast, f_S is the spatial frequency, f_T is the temporal frequency, x is spatial dimension, and t is time of the stimuli $F(x,t)$. The name of these stimuli are often referred to counter-phase stimuli [Robson 1966]. The counter-phase grating stimulus is simulated by MATLAB as Figure 2-9 where y-axis represents temporal frequency, the x-axis represents the spatial frequency, and z-axis represents the $F(x,t)$. It is an abstraction because the image in real world consisting of various spatial frequencies.

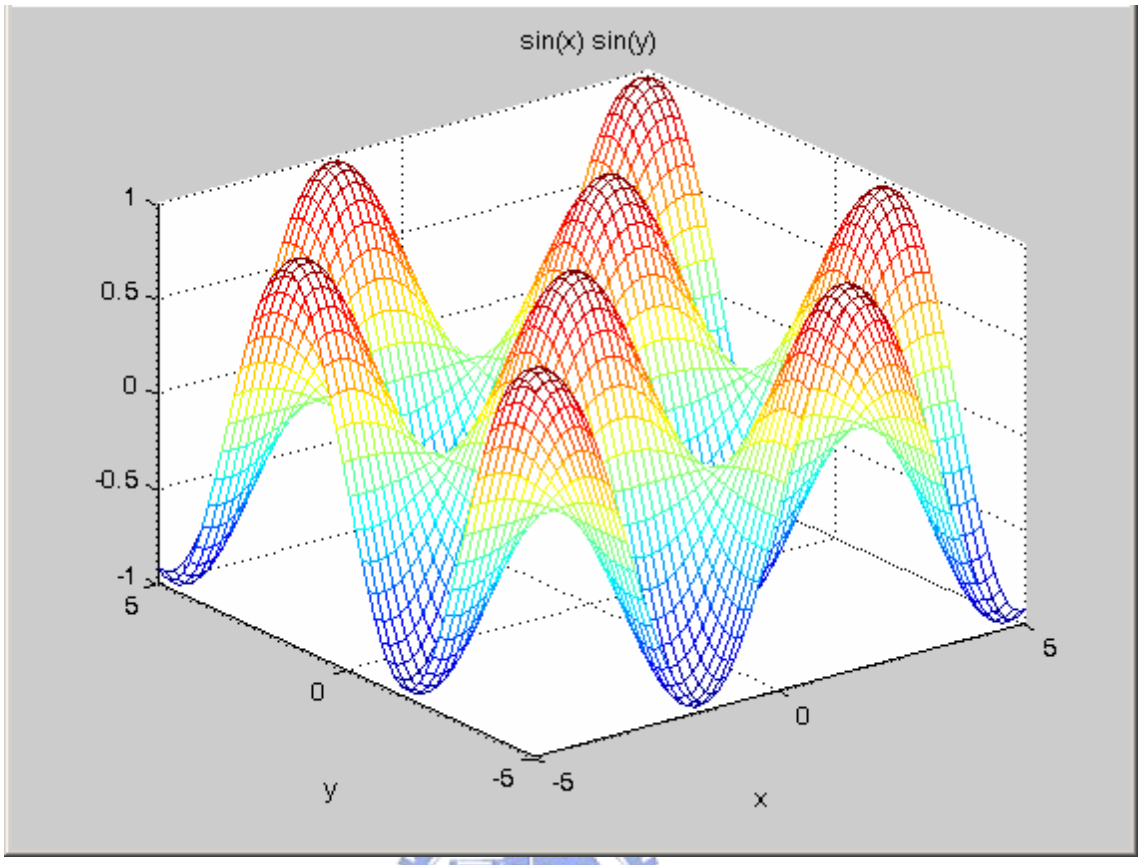

Figure 2-9: Counter-phase grating stimulus. Where y-axis represents temporal frequency, the x-axis represents the spatial frequency, and z-axis represents the intensity variation.

2.6 Eye Movements and Spatial-temporal Contrast Sensitivity Surface

At the end of 70s, Kelly considered the relationship between motion stimulus and spatio-temporal threshold surface. He found that the stabilized contrast-sensitivity function measured at a constant retinal velocity is tuned to a particular spatial frequency, which is inversely related to the velocity chosen. In the simple words, contrast sensitivity change with the relative velocity on retinal [Kelly 1979]. The stabilized stimulus is keeping the retinal image in the same position. The method of stabilizing stimulus is that display shifting the sine-wave grating by information coming from the eye tracker tracking the eye movement.

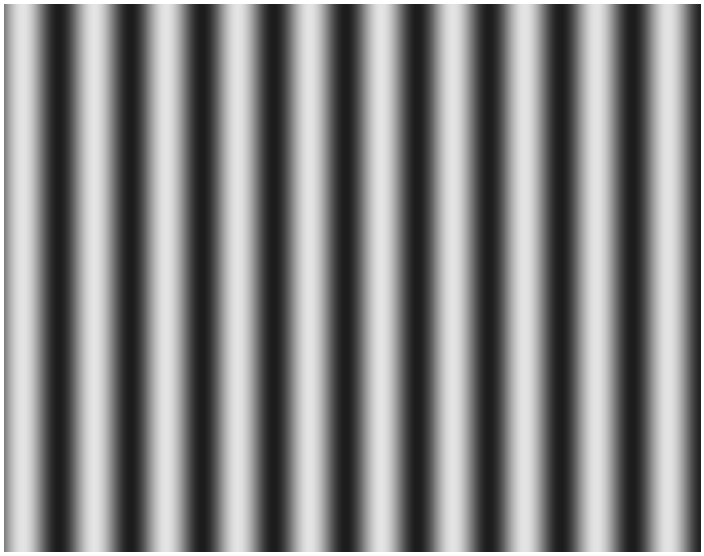

Figure 2-10: Typical Periodic sine-wave grating stimulus used as a stimulus.

When spatiotemporal sine-wave thresholds were measured under stabilized-image conditions, and plotted as a function of both spatial and temporal frequencies, the sensitivity surface is shown in Figure 2-11. Although temporal frequency is one of the independent variables in this plot, sine-wave flicker was not used to generate the stimuli. Instead, all the data were obtained with sine-wave patterns moving across the visual field at constant velocity as equation (6). It is combined the equation (7) and (8) then canceling the stationary component because the moving object has more sensitivity than stationary object.

$$F(x,t) = L(1 + m\ cos(2\pi f_S(x-Vt)\ )\ ) \tag{6}$$

Since $f_T = Vf_S$, where f_T is the temporal frequencies at a fixed point in space [Kelly 1979]. The equation of the traveling stimulus can be derived from equation (7) to (9) by trigonometric identity.

$$f_S\ (x,t) = cos(2\pi f_S x)cos(2\pi f_T t) \tag{7}$$

$$f_T\ (x,t) = cos(2\pi f_S(x-vt)) \tag{8}$$

$$2f_S\ (x,t) = 2cos(2\pi f_S x)cos(2\pi f_T t) = cos(2\pi f_S(x-vt))+ cos(2\pi f_S(x+vt)) \tag{9}$$

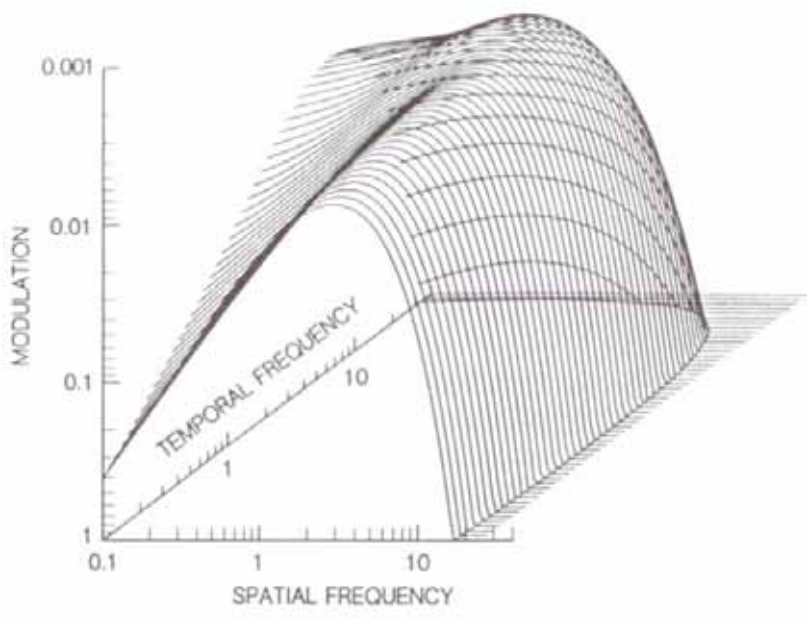

Figure 2-11: Spatial-temporal contrast sensitivity surface with smooth interpolation [Kelly 1979].

In the Figure 2-12, the curves are the contrast sensitivity at different velocities from 0.125 to 128 degree per second. The peak of curve shifted from a high spatial frequency toward to a low spatial frequency as constant velocity from low toward to high.

The contour map of spatio-temporal sensitivity surface, as in Figure 2-13, origins from Figure 2-11. Here it can be seen that the surface is almost bilaterally symmetric about a diagonal line that represents a constant velocity, $V = 2$ degree per second.

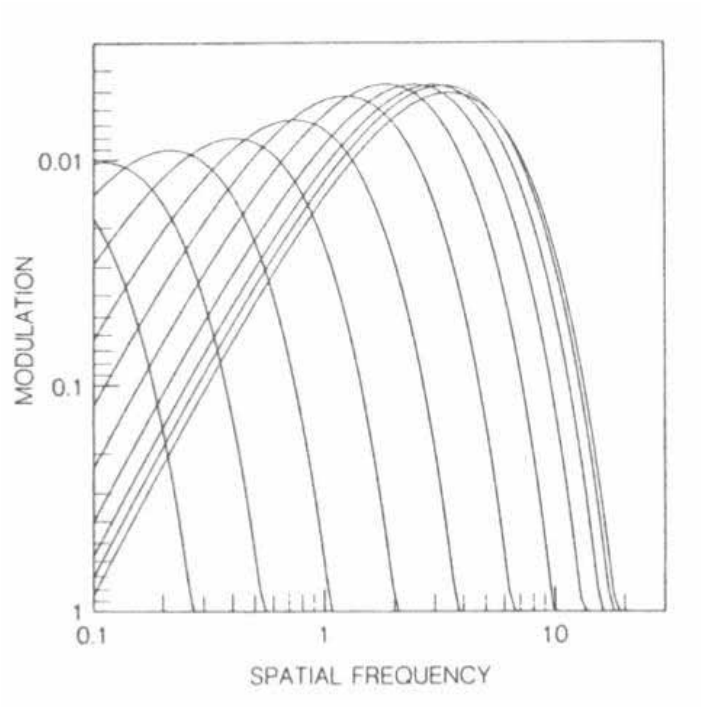

Figure 2-12: The theoretical curves of contrast sensitivity at constant velocities of 0.125, 0.25, 0.5, 1, 2, 4, 8, 16, 32, 64, and 128 deg/s [Kelly 1979].

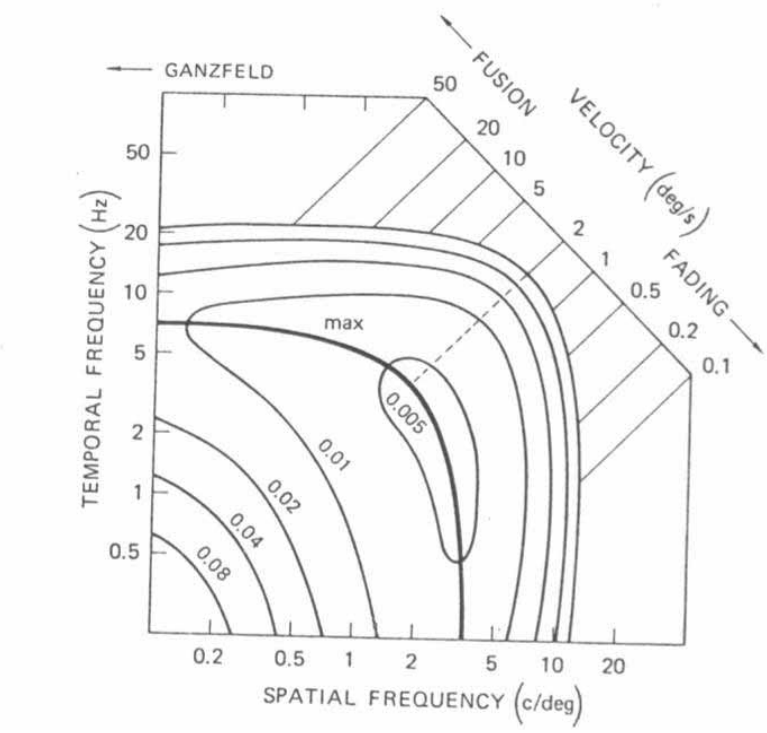

Figure 2-13: Contour map of the spatio-temporal sensitivity surface. The heavy line represents the locus of peak sensitivity at any constant velocity. The entire surface has approximate bilateral symmetry about the dashed diagonal line, *V* = 2 deg/s [Kelly 1979].

After computed-aided and trial-and-error data fitting, Kelly fitted a model to the data as the equation (10).

$$CSF(\rho, v_R) = k \cdot v_R \cdot (2\pi\rho)^2 \exp\left[-\frac{4\pi\rho}{\rho_{\max}}\right] \tag{10}$$

$$k = s_1 + s_2 \cdot \left|\log(c_2 v_R / 3)\right|^3$$

$$\rho_{\max} = p_1 / (c_2 v_R + 2)$$

Where ρ is spatial frequency in cy/deg and v_R is the retinal velocity in deg/sec. The constants are given by s_1=6.1, s_2=7.3 and p_1=45.9 and the simulated result of spatio-velocity CSF surface and contour are plotted as below:

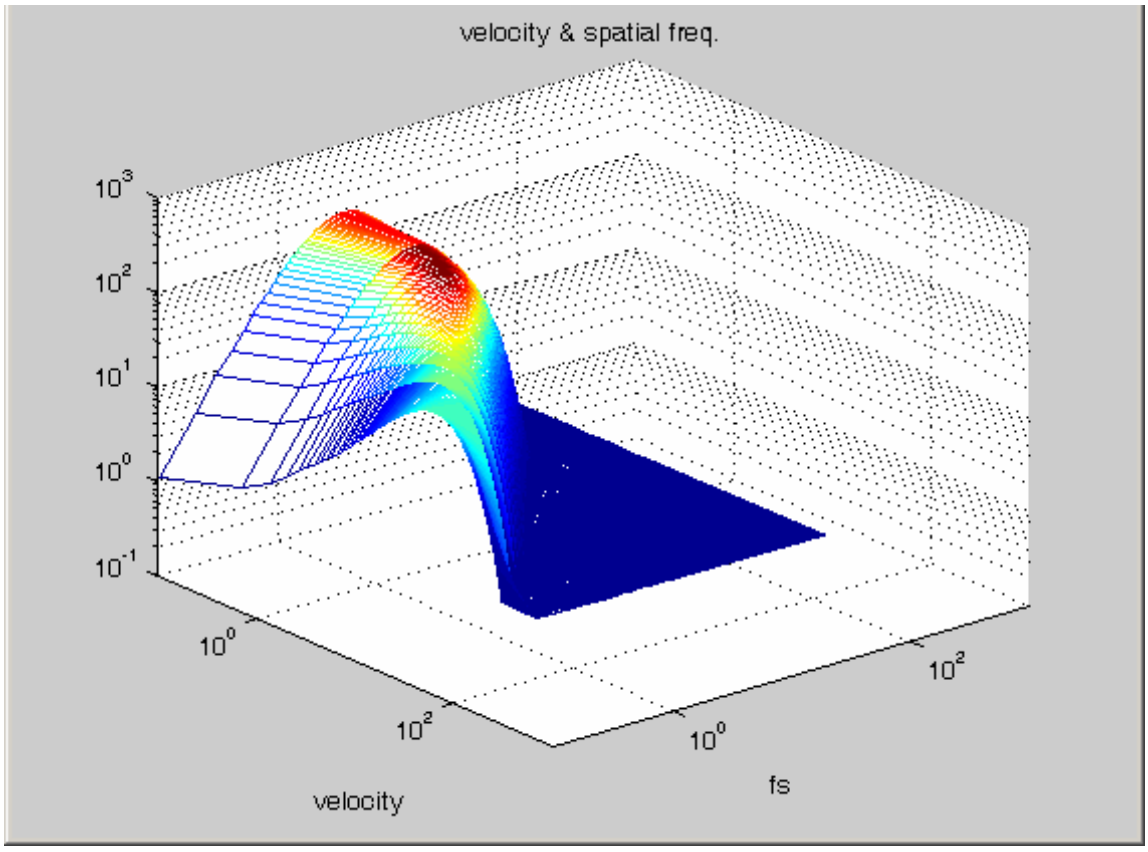

(a)

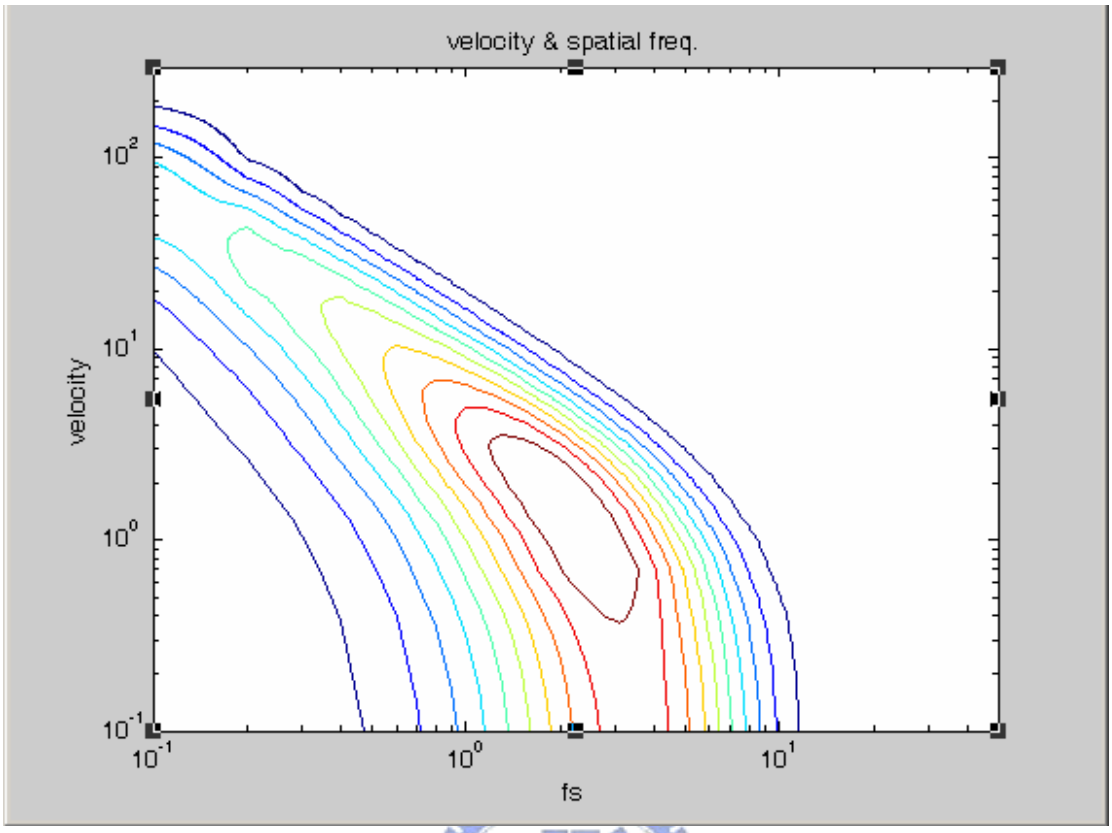

(b)

Figure 2-14: Spatio-velocity CSF surface is plotted by Matlab using Kelly's CSF model (a) and its contour plot (b).

In 2001, Daly add three constants c_0, c_1 and c_2 for modifying the model that allow fine tuning and are set to 1.0 for the original equation (10). The modified equation is described as the equation (11).

$$CSF(\rho, v_R) = k \cdot c_0 \cdot c_2 \cdot v_R \cdot (c_1 2\pi\rho)^2 \exp\left[-\frac{c_1 4\pi\rho}{\rho_{\max}}\right] \tag{11}$$

$$k = s_1 + s_2 \cdot \left|\log(c_2 v_R / 3)\right|^3$$

$$\rho_{\max} = p_1 / (c_2 v_R + 2)$$

2.7 Chromatic Contrast Sensitivity Function

In the middle of 70s, Kelly wanted to characterize the color vision mechanism by spatio and temporal sensitivity surface. The complete spatio-temporal threshold surface for each cone mechanisms is abbreviated to four critical profiles: two contrast-sensitivity curves measured at the temporal frequencies of minimum and maximum sensitivity, and two flicker-sensitivity curves measured at the spatial frequencies of minimum and maximum sensitivity [Kelly 1974].

In the spatio-temporal frequency domain, low-frequency inhibition occurs not only for white light, but also under red-, green-, and blue-selective adapting conditions. Throughout most of the spatio-temporal domain, the green sensitivity is greater than the achromatic sensitivity, the red is less, and the blue is least of all as Figure 2-15.

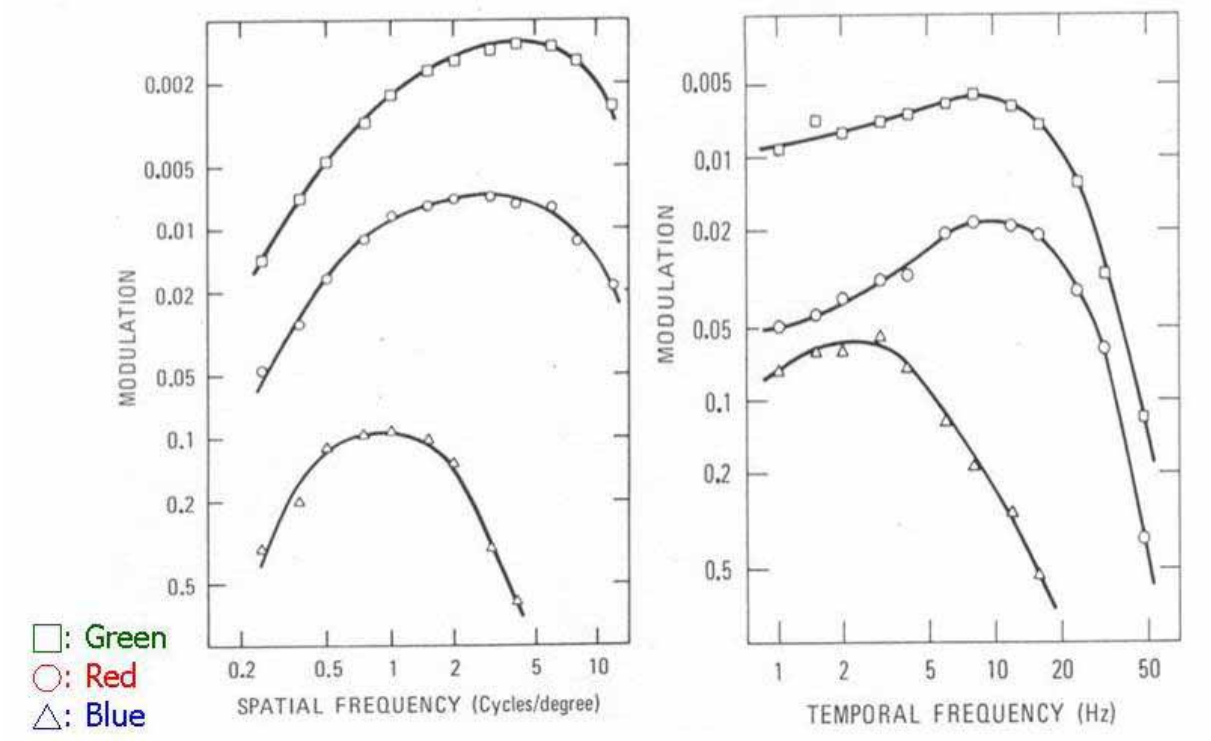

Figure 2-15: Contrast sensitivity with no flicker (left) and pattern-less flicker sensitivity (right) for the green (squares), red (circles), and blue (triangles) [Kelly 1974].

In 1977, Kelly reconciled the results of several chromatic flicker studies. By adjusting the relative amplitudes of red and green sine-wave stimuli that were flickering in opposite phase, and obtained conditions varying from purely chromatic (red-green) stimulation to

purely luminous (homochromatic) stimulation. The chromatic and luminous flicker stimuli differed only in the relative phase of their red and green waveforms, as illustrated in Figure 2-16. The purely chromatic stimulus as Figure 2-16 (a) is also named iso-luminance stimulus; and the purely luminance flicker stimulus as Figure 2-16 (b) is also named iso-chromatic stimulus.

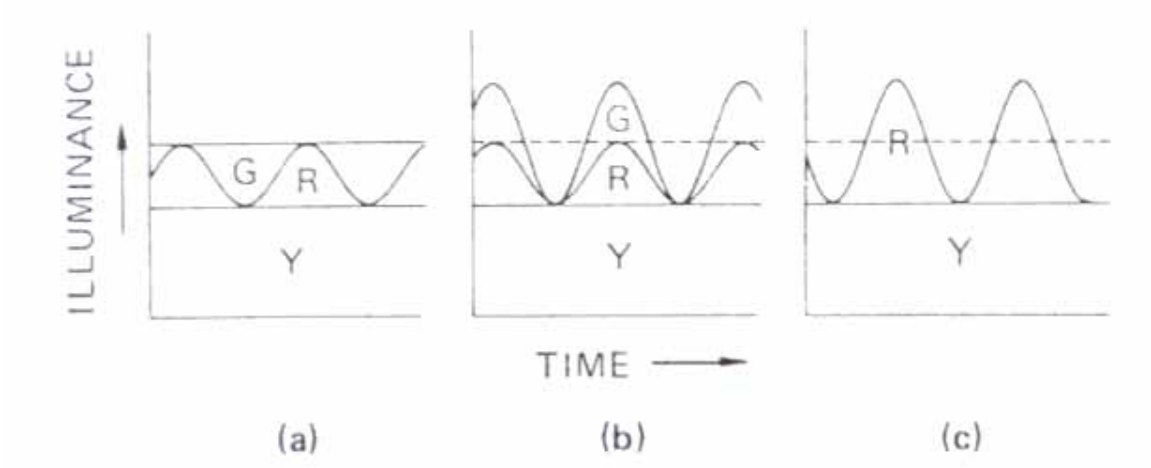

Figure 2-16: Schematic diagrams of the stimulus waveforms. (a) The purely chromatic stimulus (red-green). (b) The purely luminous flicker stimulus (yellow), these equal luminous red and green waveforms were shifted into the same phase. (c) Red stimulus with yellow background [Kelly 1977].

In next decade, Varner discovered the temporal sensitivity with the three opponent process in human visual system. Clear differences were found in observers' sensitivities to iso-chromatic luminance variations and to iso-luminous chromaticity variations for wavelength pairs selected to test temporal discriminability along the red-green and yellow-blue dimensions, respectively [Varner 1984]. The main result was that overall sensitivity for yellow-blue was less than that for red-green for all observers as below Figure 2-17.

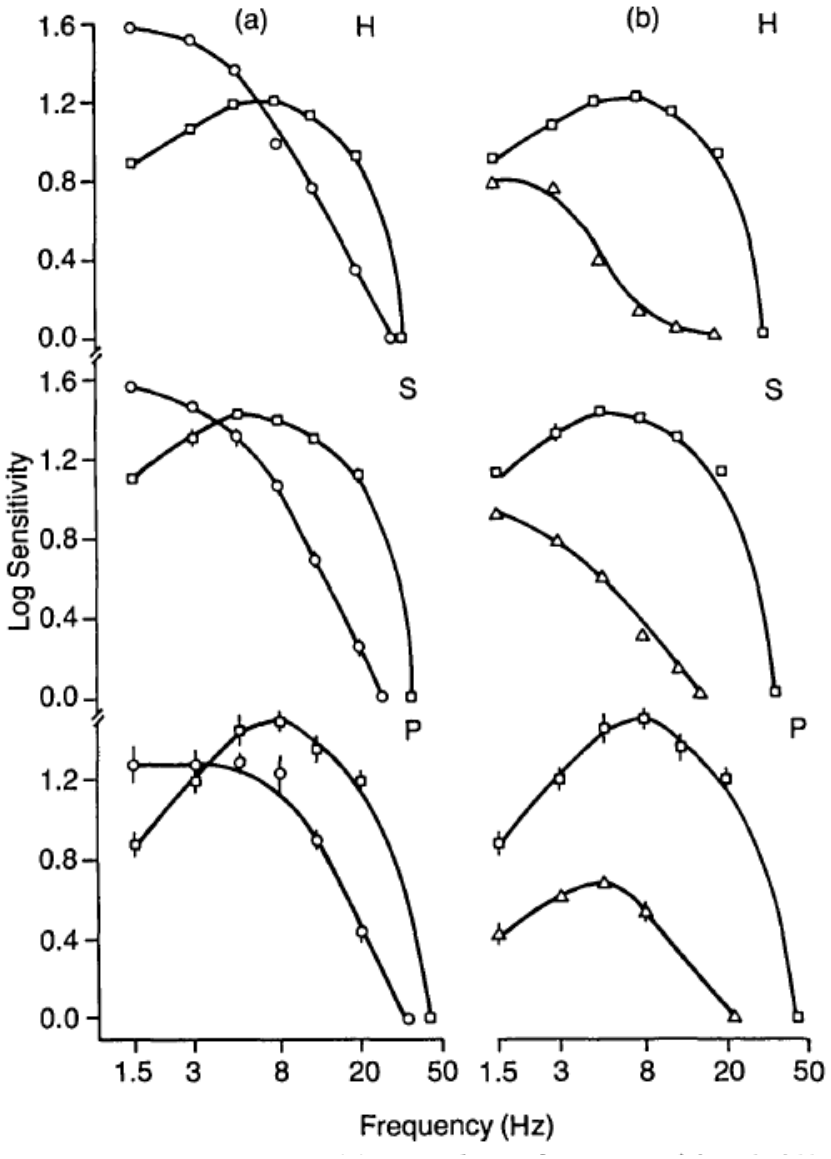

Figure 2-17: Temporal sensitivity. (a) red-green chromaticity sensitivity (open circles) and luminance sensitivity (open squares). (b) yellow-blue chromaticity sensitivity (open triangles) and luminance sensitivity (open squares). Abscissa is temporal frequency in Hz [Varner 1984].

In 1987, Swanson employed LEDs with wavelength 560nm and 630nm to produce similar stimulus as above-mention. Both mean luminance and field size affected sensitivity, and the magnitude of field-size effects increased with mean luminance. When the data are plotted in terms of amplitude sensitivity, the functions for 9 to 900 Td converge at high temporal frequencies as Figure 2-18 (top left). The temporal contrast-sensitivity functions change from low-pass to band-pass as mean luminance increased as Figure 2-18 (bottom left).

Chromatic modulation are plotted in terms of amplitude sensitivity, the 0.9 to 90 Td function converge at high frequencies as Figure 2-18 (top right). The chromatic temporal contrast-sensitivity functions show a systematic dependence on mean luminance as Figure 2-18 (bottom right).

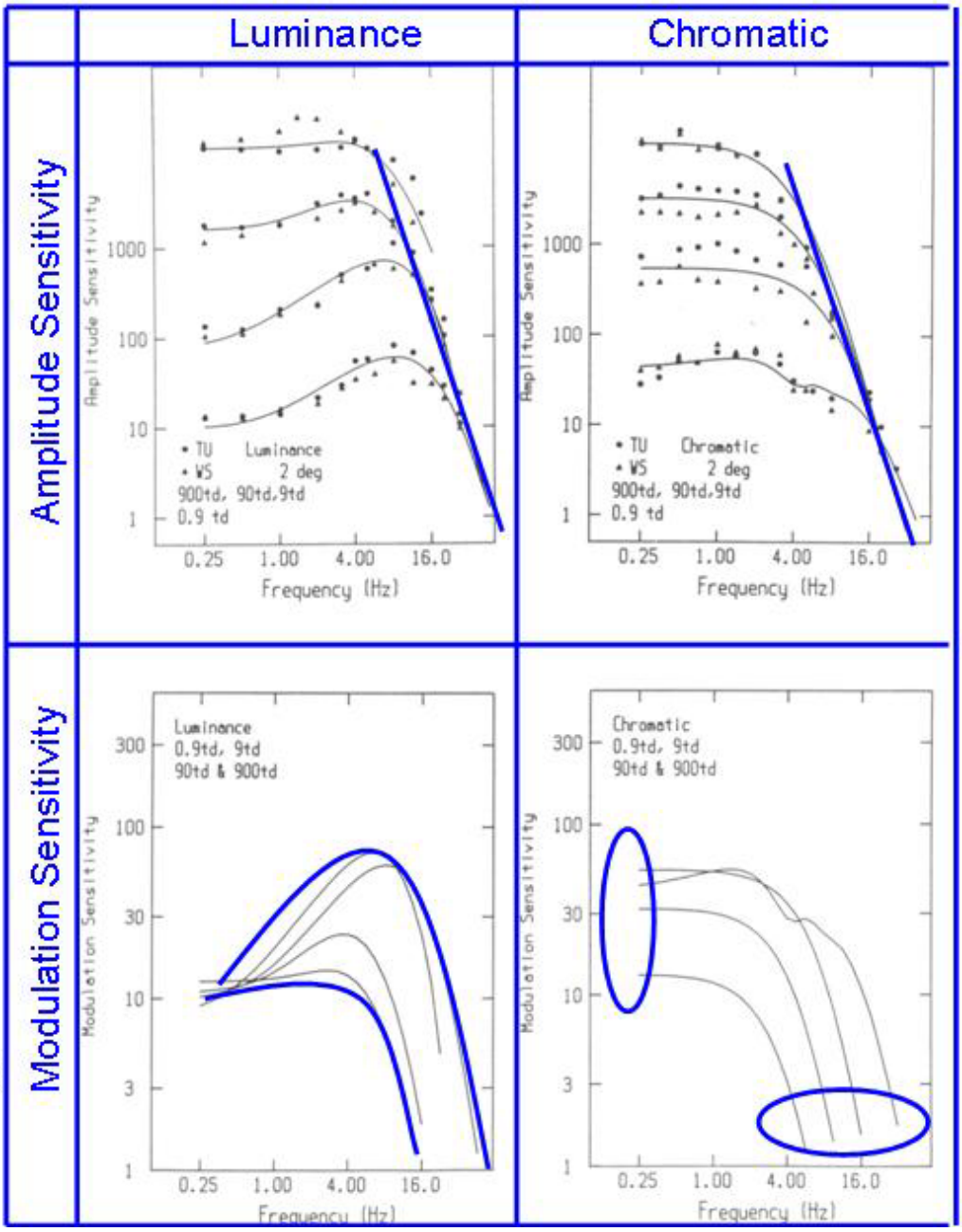

Figure 2-18: Amplitude sensitivity (top), and modulation sensitivity (bottom) was as a function of frequency for luminance (left) and chromatic (right) [Swanson 1987].

2.8 Chromatic Contrast Sensitivity Surface

In 1983, Kelly applied the contrast sensitivity surface to chromatic stimuli. The stimuli were sinusoidal, iso-luminance red-green gratings, moving across the retina at constant velocity. The luminances of the red and green channels were matched by flicker photometry [Kelly 1983]. The chromatic sensitivity surface obtained with stabilization, drifting gratings is shown in Figure 2-19. The definition used here conforms as closely as possible to the usual definition of achromatic contrast given the properties of the color CRT. Because the luminance of the green phosphor was almost twice that of the red, the two were brought into approximate iso-luminance bye viewing the CRT through a sharp-cutting orange filter. The iso-luminance condition was fine-tuned for the given subject by electronically adjusting the green contrast to a level slightly below the red. That adjustment also had to be varied with the temporal frequency of the stimulus.

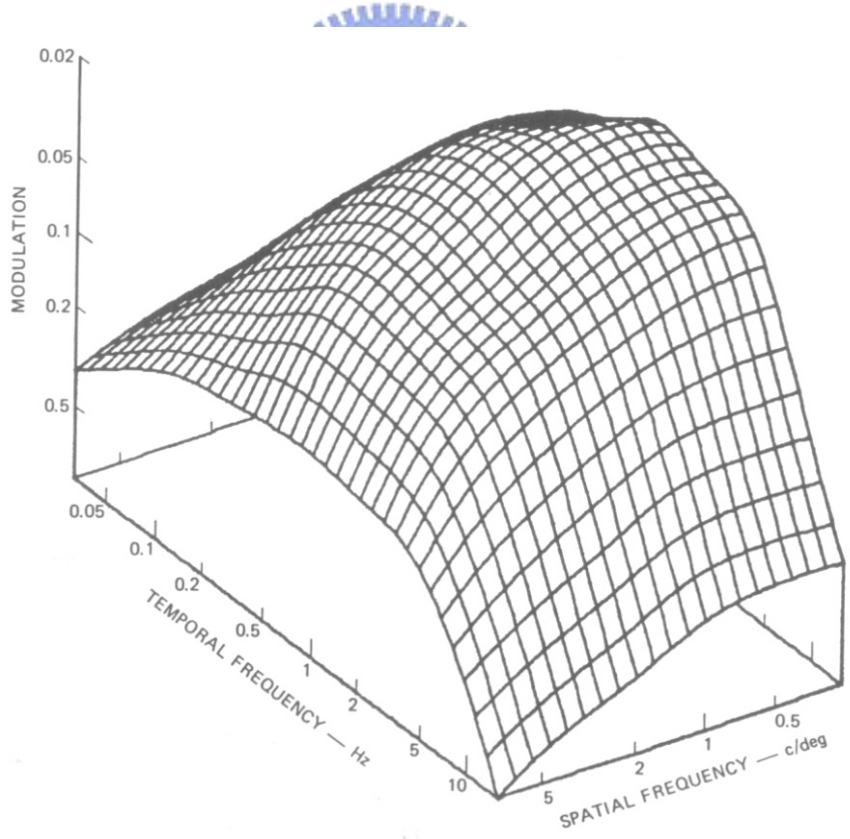

Figure 2-19: Chromatic contrast sensitivity surface measured with red-green, iso-luminance, drifting sinusoidal gratings [Kelly 1983].

2.9 Field Sequential LCDs

The field sequential liquid crystal displays (FSLCDs) technology synthesizes color by employing the additive property of Grassmann's law and temporal properties of human visual system. The color filter is completely eliminated, giving three times luminance advantage, and the number of column lines is a factor of three lower than for the conventional LCDs. However, there is a significant visual effect color breakup, also named rainbow effect, because of a color pattern might be seen [Arend 1994].

Despite the intrinsic advantages of color sequential LCDs, implementation in color sequential LCDs has been held back by lacking fast-response liquid crystals (LC), high cost and low luminous efficiency of non-white LEDs, moderate need for high resolution displays with wide gamut, and poor visibility in ambient light. Recently, however, there is an increased interest in wide-gamut, high-information content mobile displays. Fast liquid crystals such as optically compensated bend (OCB) have been implemented in LCDTV [Yamagishi 2006] and highly saturated LEDs with high luminous flux have been successfully developed.

Although the faster liquid crystals response like OCB have been developed to improve the response time, this kind of liquid crystals is not available to all of the LCD manufactures and have some drawbacks like demanding extra compensation films for improving the dark image [Lee 2006].

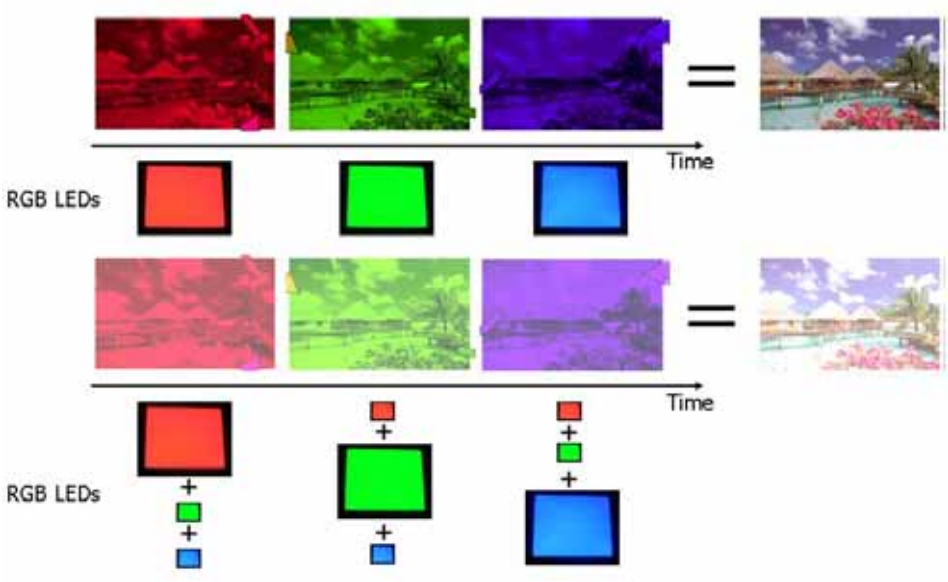

Figure 2-20: Compare the color sequential LCD paradigms between the conventional method (top) and the color breakup reducing method (bottom).

The conventional color sequential LCDs with LED backlight divides a frame into 3 sub-fields including the R, G, and B-field with color breakup when the refresh rate is not fast enough. If we have already known one image is not saturate, we could introduce color crosstalk intentionally to LED backlight as shown as Figure 2-20 [Sun 2006].

2.10 Summary

Many temporal properties of human system are discovered in the past century. Both Broca-Sulzer effect and Brücke-Bartley effect can increase the perceived brightness. Broca-Sulzer effect states that the flashing light at low duration (50-100 milliseconds) appears brighter than shorter or longer duration light. Brücke-Bartley effect illustrates that the light modulated (flickered on and off) at low frequency (5 to 20 Hz) appears brighter than lower or higher frequency light. For applying these properties to the low power LCD, psychophysical experiments are performed to model the relation between perceived brightness and flickering frequency. Base on the experimental results, a novel backlight driving scheme will be proposed.

Chapter 3

RGB LED Backlight Module

Currently, most of the backlight modules of LCD for laptop, PC and TV monitors are dominated by *cold cathode fluorescent lamp* (CCFL). However, the CCFL has three main problems including narrow color gamut, long response time, and mercury contained even through it is cost efficiency. To solve these problems, the *RGB light emitting diode* (LED) backlight module has been proposed for its features such as fast response, wide color gamut, and mercury-free. A LED backlight consists of light-bars with a number of RGB LEDs, which are semiconductor devices emitting light when electrical current flows through it forwardly.

Although LEDs can be applied to LCD backlight, it has disadvantages such as power efficiency, color light mixing distance, electro-optical characteristic variation among LEDs, temperature dependency of color and luminance and high cost. How to minimize these shortcomings must be considered in the design process. An RGB LED backlight module with dimming control was fabricated and its characteristics are compared with those of CCFL in this chapter.

3.1 Specification

This backlight module has the features as below:

- Three primaries including red, green, and blue light
- Red light has a peak wavelength at 631nm, green light has a peak wavelength at 535nm, and blue light has a peak wavelength at 460nm
- Color gamut is larger than 120% of NTSC in the CIE x-y coordinate

- Fits 19-inch screen (376 mm × 307 mm)
- Maximum luminance is 5000 cd/m^2
- Dimming control by pulse width modulation signal
- Edge lighting backlight module

3.2 Block Diagram

The aim of this RGB LED backlight module is to replace CCFL directly without changing any mechanical parts. In Figure 3-1, on the left is a traditional LCD with CCFL backlight, and on the right is the re-designed LCD with LED backlight. The backlight module employed the LED driver instead of the inverter used for CCFL backlight. Different from CCFL backlight, there are three dimming control signal for LED backlight. Therefore, the LED backlight is able to dim red, green, and blue separately.

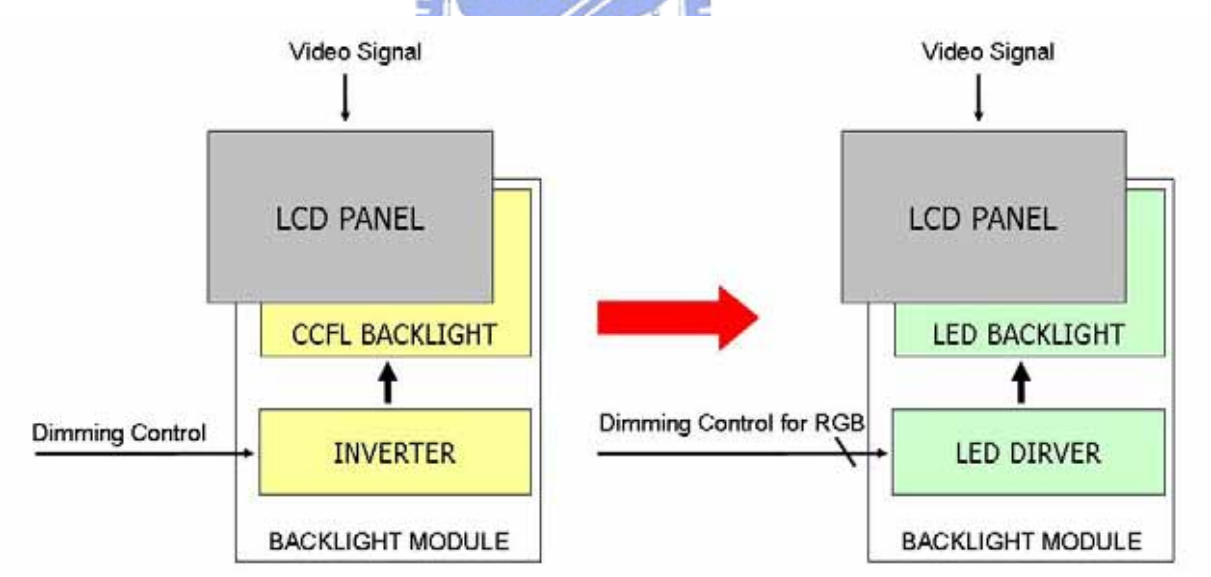

Figure 3-1: The CCFL backlight and inverter (yellow block) are replaced by RGB LED back light (green block).

3.3 Backlight Module Design

In the backlight module design flow, there are three major considerations: optical design,

thermal issue, and electrical design [Anandan 2006].

First, a 19” LCD monitor (ViewSonic VX912) is reworked as a prototype for measuring the relation between luminance and electric current. Two lightbars, each with 24 LED chips, take place of the original CCFL backlights inside the LCD monitor. One was put on the top edge and the other at the bottom. Close-ups of a LED chip and lightbars are shown in Figure 3-2.

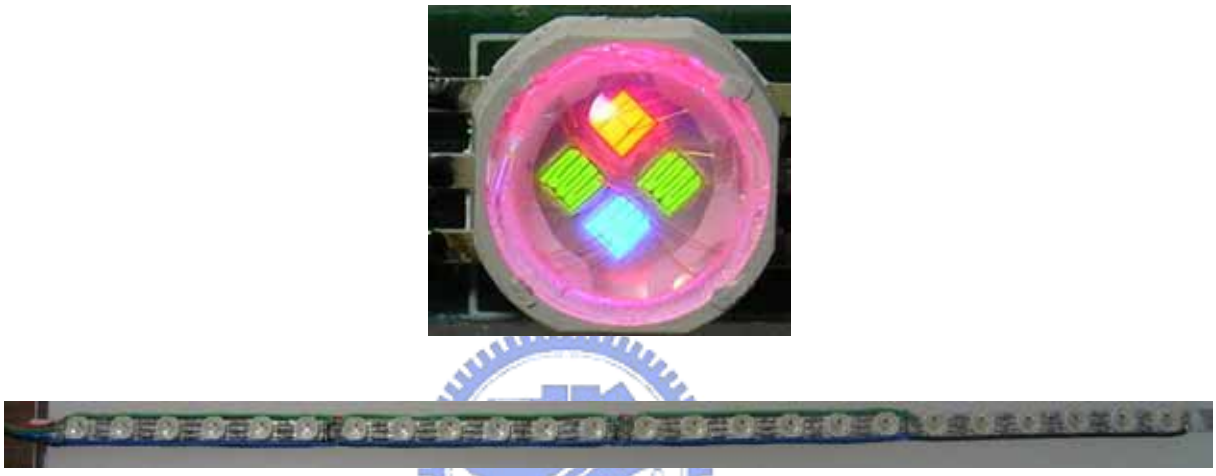

Figure 3-2: Close-up of LED chips with one red die, one blue die and two green dies (top) and LED light-bar with 24 LED chips (bottom).

This prototype worked as a traditional backlight after been powered by power supplies. The electrical current flowing through the prototype and the corresponding luminance were measured and recorded. Based on the data, we calculated the power consumption of each LED.

Three-in-one (three primary colors in one package) RGB LEDs (Arima Optoelectronics Corporation 5WRGGB) were chosen to minimize the light mixing distance [Zwanenburg 2004]. The benefits of the three-in-one LED is that because the chips are all integrated in a single package, the light is essentially mixed within the package. Hence, there is no additional space required to achieve uniform color mixing. As shown in Figure 3-3, using discrete RGB LEDs with 10 mm pitch and three-in-one LEDs, the color-mixing distance is reduced from 28mm to 7mm.

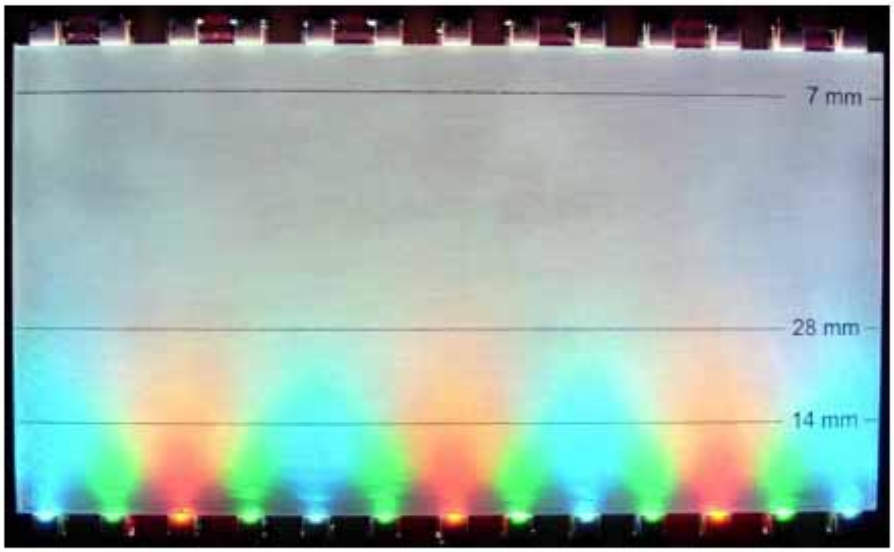

Figure 3-3: The snapshot of color-mixing distance of the backlight module: comparison between three-in-one RGB LEDs (top) and discrete RGB LEDs (bottom) [Zwanenburg 2004].

Second, when more and more electrical current flows through LEDs, the LED lightbar becomes hotter and hotter because LEDs translated a lot of the electrical power into heat. After the critical temperature point, the blue light declined firstly and dramatically. The amount of the electrical current was the upper limit for the LED driver. To prevent dissipate heat from the light-bar, the heat sink compound was applied to the gap between the thermal pads of LEDs and the lightbar. Furthermore, the lightbars must contact the metal frame tightly to improve heat dissipation.

Figure 3-4: The heat sink compound which was applied between the thermal pad of LEDs and the light-bar.

In the last step, the LED driver was the most important part in the LED backlight module.

A number of electrical circuits for driving LED are available. For efficiency and stability, current mirror was chosen as LED driver because it can supply stable constant electrical current and adapt to different forward voltages of each LED. It is very suitable for driving LED because the output luminance is a function of the forward current through LEDs.

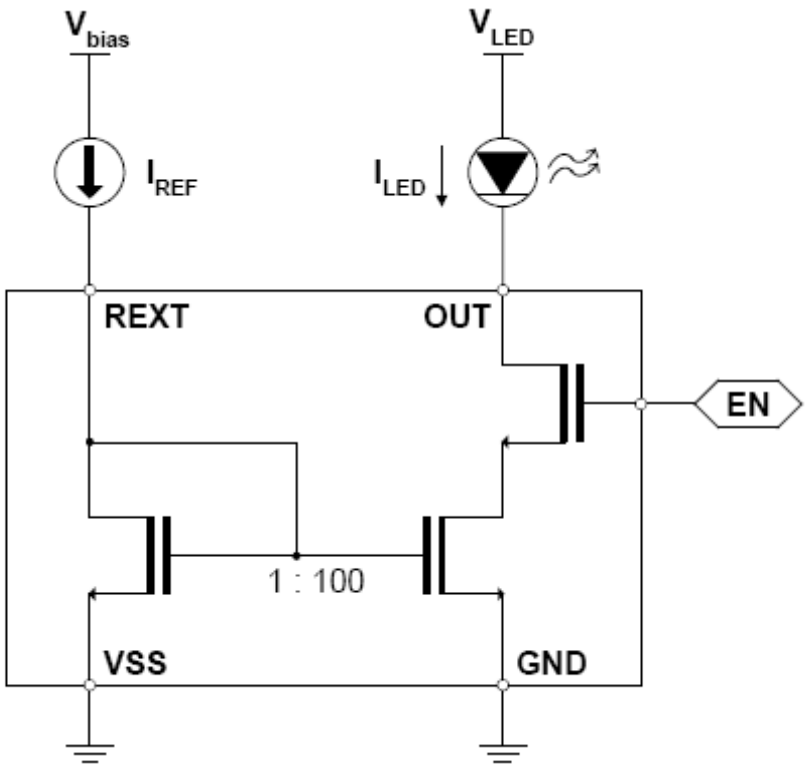

Figure 3-5: The current mirror circuit with one hundred times current output provides a constant current for LED and is adjusted by changing I_{REF} [SiTI].

Figure 3-5 shows a general current mirror. I_{LED} is the constant LED forwarding current which is one hundred times the reference current I_{REF}. The output light can be turned on by ascending the enable (EN) pin to high voltage level and turned off by descending the EN pin to low voltage level. The LEDs' intensity can be controlled by adjusting the amount of I_{REF} via an external circuit.

In this backlight module, a high constant current mirror (Silicon Touch Technology DD311) was chosen as the LED driver because it can sustain up to one ampere forward current. It is a single-channel constant current LED driver incorporated current mirror and

current switch. The maximum sink current is 100 times the input current value set by an external resistor or bias voltage. The maximum output voltage of thirty-three volts can provide more series power LEDs in a string. The output enable (EN) pin allows dimming control or switching power applications [SiTI].

Based on the thermal and optical design mentioned above, the maximum forwarding current of LEDs can be determined so that the reference current can be derived by dividing one hundred. The LEDs' voltage supply V_{LED} can be determined by calculating each LED's V_{TH} in series connection.

3.4 Implementation

The implementation flow of LED backlight module consists of seven steps as illustrated in Figure 3-6.

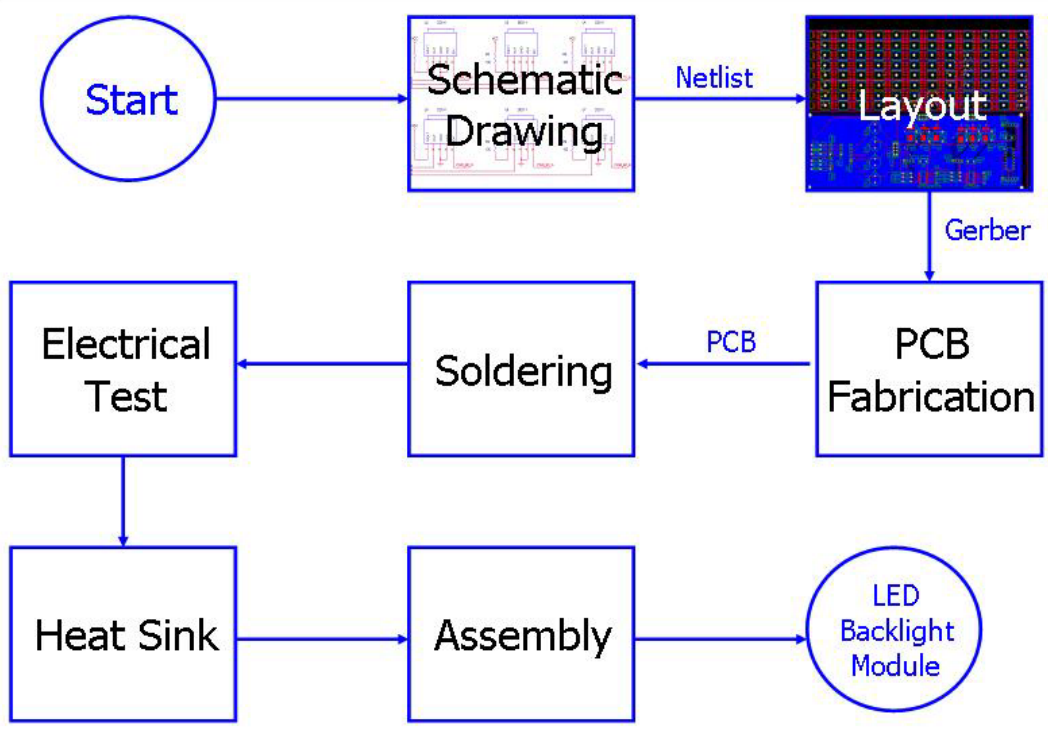

Figure 3-6: From start to LED backlight module, the implementation flow consists of seven steps: schematic drawing, layout, PCB fabrication, soldering, electrical testing, heat sink assembling, and mechanical assembling.

The first step is schematic drawing, assisted by the software OrCAD® Capture, a design tool of Cadence®. The LED driver, LED lightbar, and other electrical components were designed by schematics. Two of the schematic designs are shown in Figure 3-7.

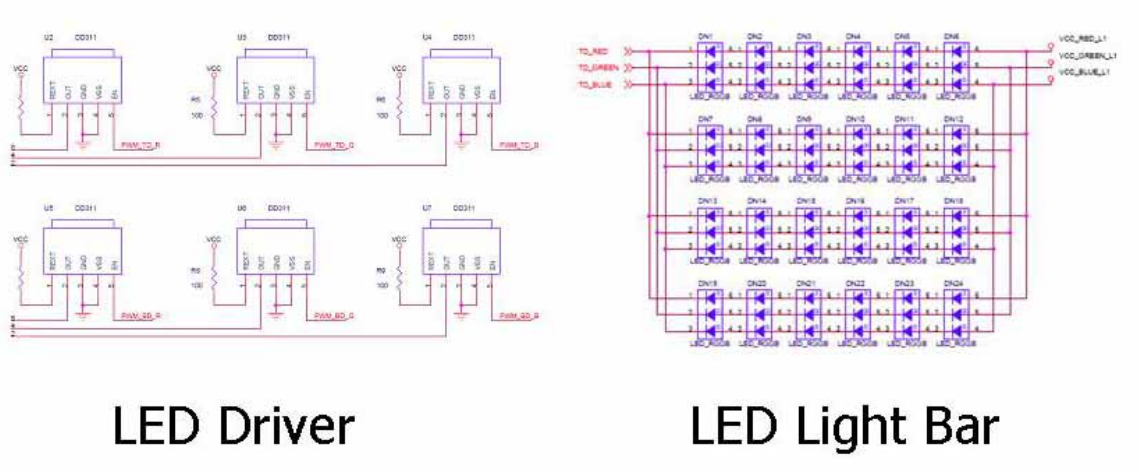

Figure 3-7: Two parts of the electrical schematics are consists of six LED drivers (left), and twenty-fore RGB LEDs (right).

The exported net-list file (*.NET) is a text file with information including the parts and the connections between blocks. Te layout step is to physically place the components and connections on a printed circuit board (PCB). In this stage, the computer-aided design (CAD) tool PROTEL® SE was employed to plot the physical outline of electrical components and the location on the PCB. Here the design rules must be observed including board size, layers, thickness, trace width, medium material, etc. The layout of LED driver and lightbar are plotted in Figure 3-8.

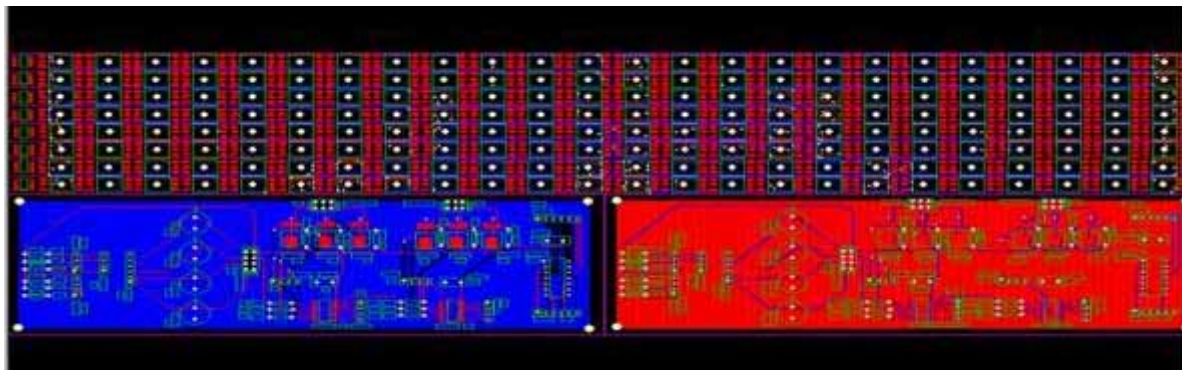

Figure 3-8: The PCB layout consists of eight strips of LED light-bar (upper), and two LED driver boards (bottom).

In the next step, layout drawing was translated into the GERBER file, a format of negatives for PCB fabricating. Bare PCBs were turned around after a week from the PCB plant. The sample bare PCB was shown on the top-left of Figure 3-9, and on the top of Figure 3-10.

The returned bare PCBs were tested for open-short, grounding and correct via. The PCB must be re-fabricated if any test failed. Before the soldering stage, each LED was tested for proper function. A lot of check items should be done because de-soldering will spend more effort than soldering. The emitting test of LEDs is shown as the top-right in Figure 3-9 and the soldering process in the bottom-left. At this stage, as the menu recommended, the hand soldering should be with a solder tip temperature of 230°C for less than ten seconds. Long soldering might cause the damage to the epoxy layer and short circuit in the array.

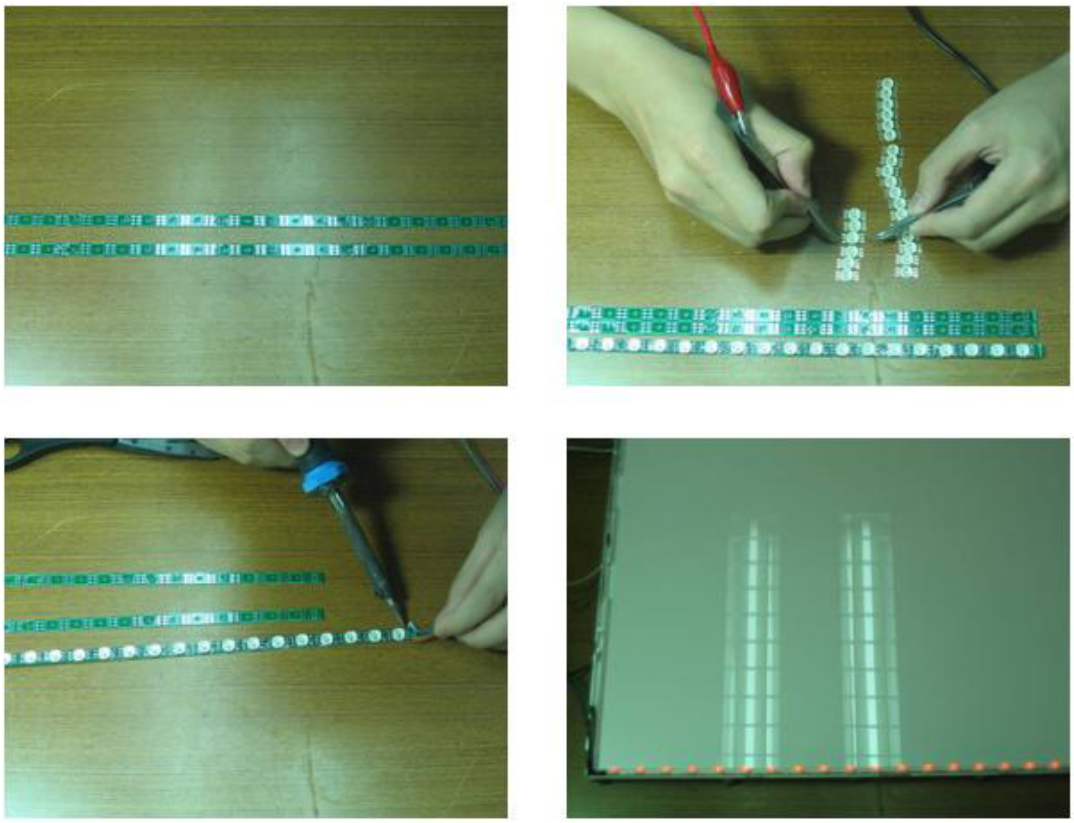

Figure 3-9: The bare PCBs of LED light-bar (top-left), LED testing (top-right), soldering process (bottom-left), and after assembling and emitting red light (bottom-right).

After the soldering stage, the LED light-bar should be connected directly to DC power supply and checked whether each LED emitted well as shown in Figure 3-9 bottom-right. Some LEDs could not emit because of “cold solder joint.” This poor property usually occurs when the base metal is not warm enough to melt the solder. When it occurs, re-soldering each metal pin of LEDs with higher temperature is better than soldering more tin on the metal pin, but it might cause lower light efficiency or de-saturation.

For thermal dissipation, the LED light-bar reserved dissipated hole for each LED. The heat sink compound mediated between the thermal pad of LEDs and the metal frame so that the LEDs dissipated heat from the thermal pad of LEDs through heat sink compound to the metal frame. However, more electrical current might cause thermal damage.

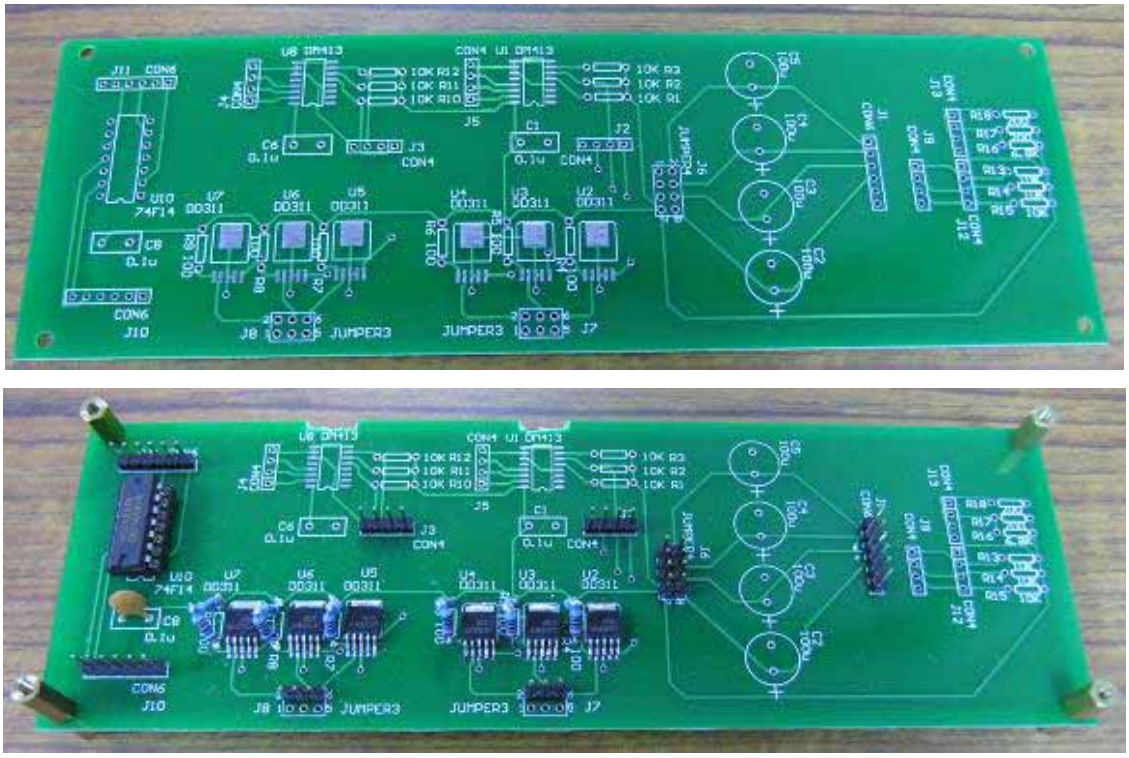

Figure 3-10: The bare PCB (upper), and the PCB with LED driver soldering (bottom).

In the LED backlight module, there are two light-bars, each one with twenty-four chips of RGB LEDs. One is on the top side; the other is on the bottom side. In LED driver board, six DD311 chips are used for two light-bars and each one with an independent enabled control.

These six chips would be divided into two groups. One group controls red, green, and blue for the top light-bar. The other controls the red, green, and blue light for the bottom light-bar. Therefore, this backlight module has ability to be used for spatial backlight scaling when an image with different color or luminance on the top and bottom side.

In the final fabricating stage, the light-bars were assembled and connected to the LED driver board, and then the RGB LED backlight module was accomplished. As shown in Figure 3-11, the LED backlight module can illuminate white, red, green, and blue with dimming control. The white point can be adjusted by the reference current of LED driver or the duty cycle from the external pulsed width modulation (PWM).

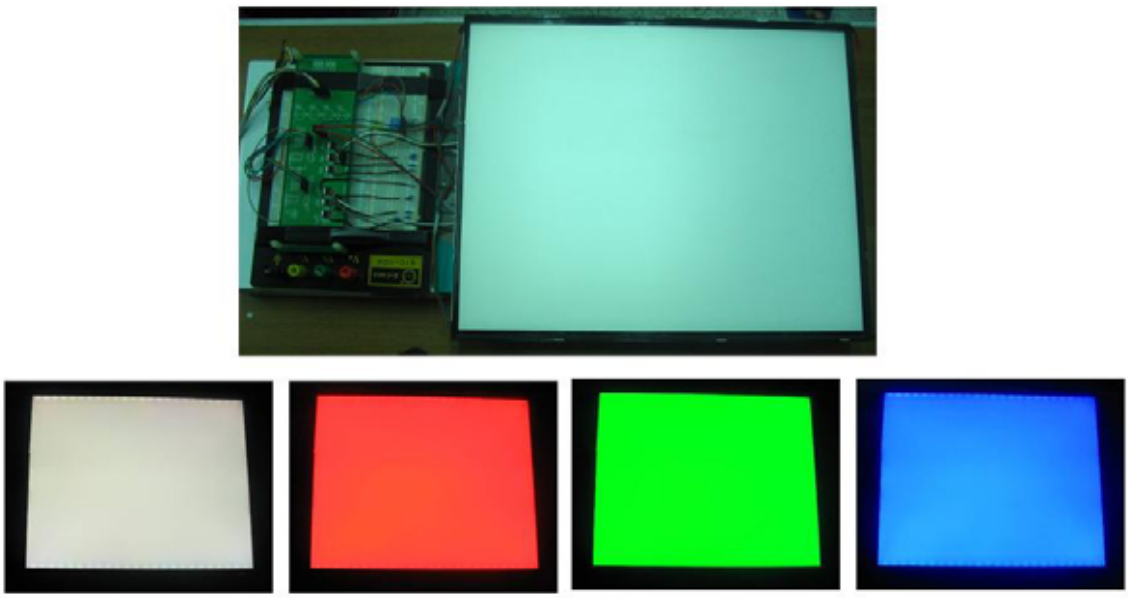

Figure 3-11: The snapshots of RGB LED backlight module (top) and emitting white, red, green, and blue light (bottom).

3.5 Calibration

Before the LED backlight module is used as an illuminator of LCD, the white point must be calibrated. The aim is to illuminate white with CIE 1931 x-y coordinate value at (0.33, 0.33) which is also named equi-energy stimulus S_E, just as $X = Y = Z$. There are two approaches to adjust the white point: the first one is dynamically modifying the duty cycle of

each color, and the other one is statically modifying the reference current by high precision resistor. The second approach is more desired because it provides better stability and precision. However, the first one is also useful in dynamic compensation for thermal problem. In the backlight module, it employed a bread board because exchanging external resistors is more convenient. After calibration progress, the value of external resistors for each color channel should be certain.

3.6 Performance of Backlight Module

We measured both the power consumption of LED and CCFL backlight, as shown in Table 3-1. The power consumption of backlight module includes driving circuits like the current-mirror circuits for LEDs or the inverter for CCFL. Both power and luminance were measured simultaneously and listed in the second and third column. In the last column, the quotient is luminance divided by power; the LED backlight illuminates more light than CCFL per watt. It is because the LEDs have higher light efficiency [Arima].

Table 3-1: Power efficiency of LEDs and CCFL

Backlight	Luminance (nit)	Power (W)	L/P (nit/W)
LEDs	4739.24	21.20	224
CCFL	4384.50	23.17	189

The spectral emission characteristics of the LED backlight module are measured with ConoScope [ConoScope] and the waveforms are shown in Figure 3-12. The red had a peak at 631nm, the green at 535nm and the blue at 460nm. The equal-energy white point (0.33, 0.33) is shown in Figure 3-12 (d), of which consists the waveform of red, green, and blue.

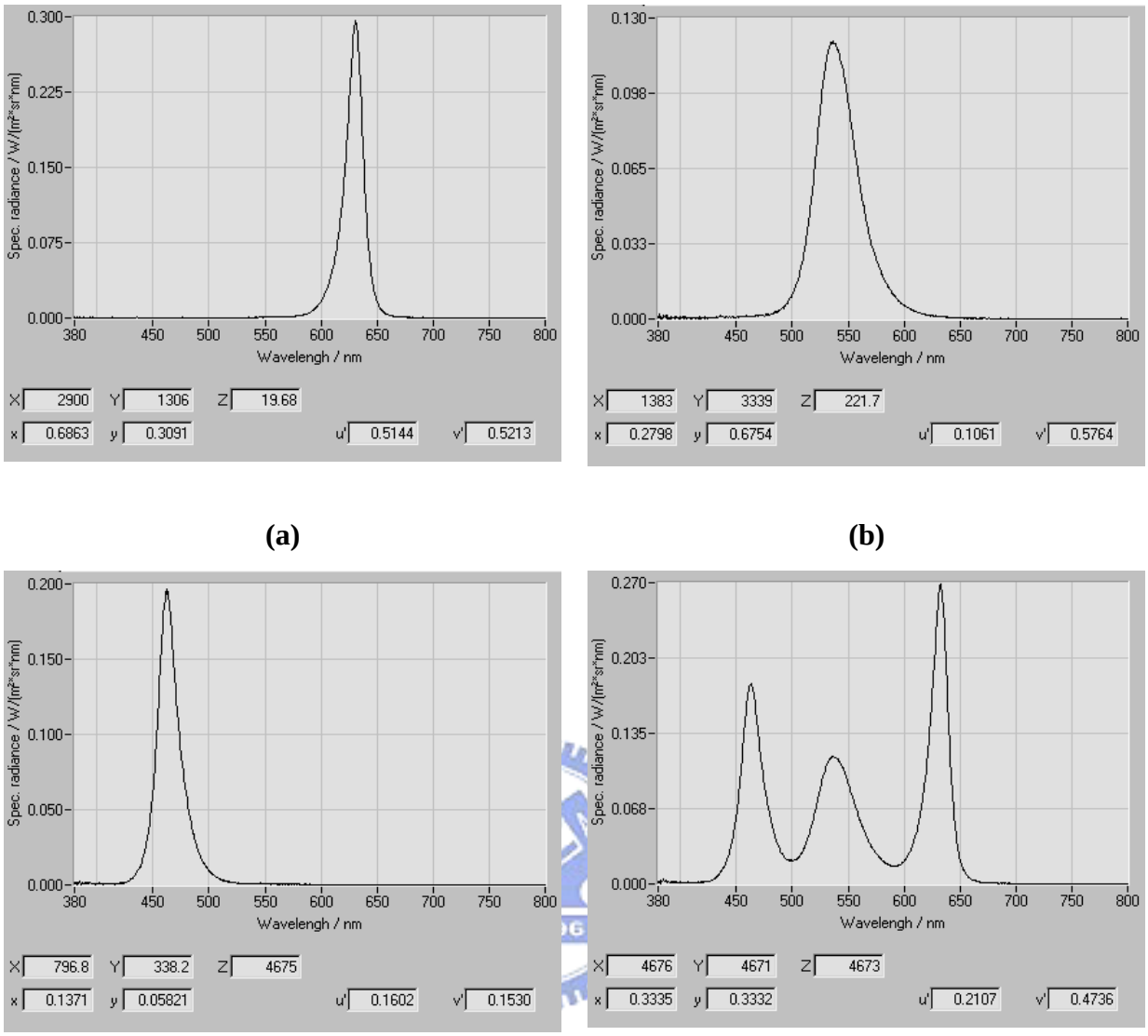

Figure 3-12: The spectra of RGB LED backlight: (a) Red LEDs had peak at 631nm. (b) Green LEDs had peak at 535nm. (C) Blue LEDs had peak at 460nm. (d) White light at x-y coordinate (0.33, 0.33).

Furthermore, the color gamut can be calculated by the triangular area formula as below:

$$S = \frac{1}{2}\begin{vmatrix} x_1 - x_3 & y_1 - y_3 \\ x_2 - x_3 & y_2 - y_3 \end{vmatrix} \tag{12}$$

Where S is the area of a triangle which three apices are coordinates of red, green, and blue respectively. The area of each color triangle is calculated and listed at fifth column in Table 3-2. The results of LEDs comparing with CCFL, NTSC and EBU specification are

listed in Table 3-2 and plotted triangles on CIE 1976 uniform coordinate u'-v' as Figure 3-13. Obviously, the color gamut of LED backlight is up to twenty percent higher than NTSC, even higher than CCFL backlight for around forty percent, because the LED backlight improves greatly in red and some in blue from CCFL triangle, as shown in Figure 3-13.

Table 3-2: Color gamut comparison

		u'	v'	Area	NTSC Ratio	EBU Ratio
NTSC	RED	0.48	0.53	0.074	100%	
	GREEN	0.08	0.58			
	BLUE	0.15	0.2			
EBU	RED	0.45	0.52	0.066		100%
	GREEN	0.12	0.56			
	BLUE	0.18	0.16			
CCFL	RED	0.43	0.53	0.061	81%	92%
	GREEN	0.11	0.57			
	BLUE	0.16	0.18			
LEDs	RED	0.52	0.52	0.089	120%	136%
	GREEN	0.11	0.58			
	BLUE	0.16	0.14			

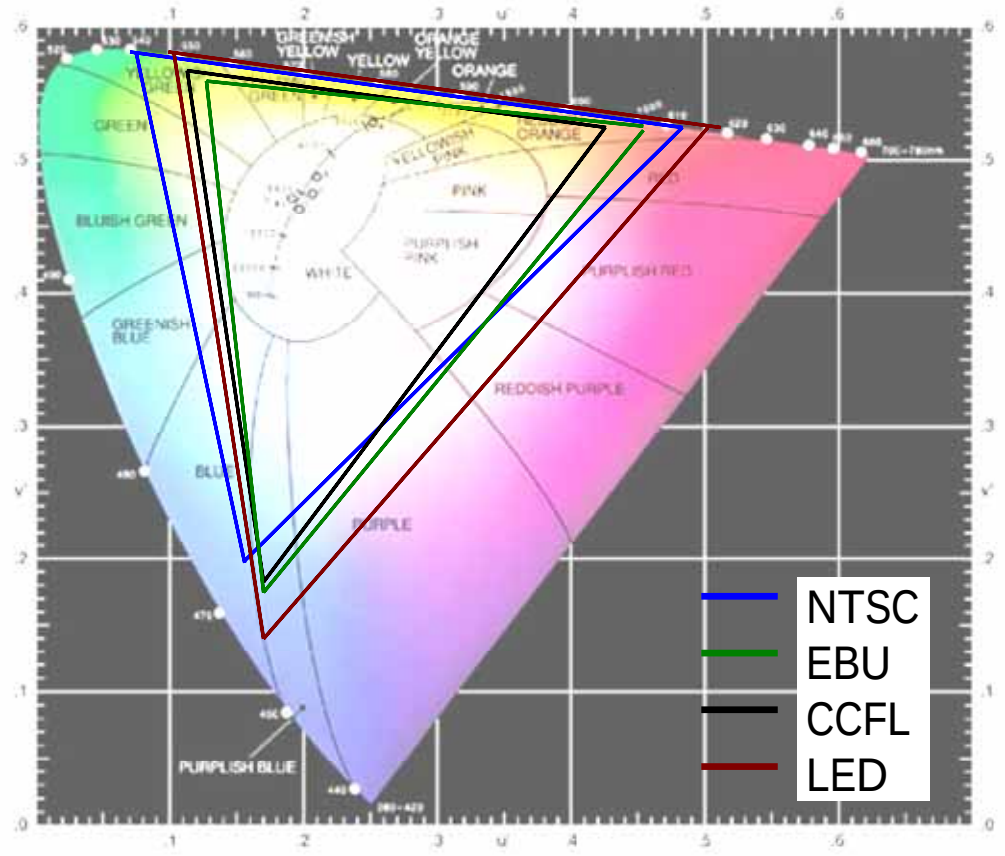

Figure 3-13: CIE 1976 u'-v' coordinate comparing color gamut of LED backlight with the CCFL backlight, NTSC specification, and EBU specification. The blue and the green triangles indicate NTSC and EBU standard, respectively. The deep red triangle indicates LED color gamut that is larger than the triangle of all the others.

3.7 Summary

A RGB LED backlight with dimming control has been fabricated through the optical, mechanical, and electrical design. The problems like color mixing, thermal dissipation, and dimming control were conquered by modern techniques. After chromatic calibration, the characteristics of LED backlight are measured and compared with CCFL backlight. Based on the measured results on the prototype, the RGB LED backlight has better light efficiency, larger color gamut, and better dimming controlled by PWM then CCFL backlight. Its characteristics were conformed to the specification defined in previous section. Therefore, this was suitable to be the backlight module for the experiments.

Chapter 4

Principle

4.1 Terminologies

Luminance is a physical measure defined as cd/m^2. The luminance of an object can be measured by a luminance meter.

Brightness is the attribute of a visual sensation according to which an area appears to emit more or less light.

Lightness is the brightness of an area judged related to the brightness of a similarly illuminated area that appears to be white or highly transmitting.

Brightness and lightness are psychophysical terms and cannot be measured by instruments. Intuitively speaking, brightness represents the perceived luminance when there is only one single color in sight, while lightness represents the relative brightness of the color when the reference white is also present [Wyszecki 1982].

4.2 Backlight Luminance Scaling

The luminance of an LCD, L, is the product of the backlight luminous intensity b and the panel transmittance t. One can decrease the backlight luminous intensity to save the power consumption. The panel transmittance should be increased accordingly such that the luminance remains the same. In addition, for LCDs, higher transmittance can reduce the light leakage problem of liquid crystals and increase the image quality in terms of color saturation and viewing angles.

Consider a pixel consisting of red, green, and blue sub-pixel. Its color is determined by the product of the backlight luminous intensity (b_w) and the transmittance of each sub-pixel (t_R,t_G,t_B):

$$\begin{bmatrix} L_R \\ L_G \\ L_B \end{bmatrix} = b_W \cdot \begin{bmatrix} t_R \\ t_G \\ t_B \end{bmatrix} \tag{13}$$

L_R:L_G:L_B is the luminance ratio of red, green, and blue. For example, white is obtained at the ratio of 0.27:0.67:0.06. An LCD generates different colors by changing the transmittance ratio of sub-pixels t_R:t_G:t_B. By increasing (t_R,t_G,t_B), one can lower b_W to save power and preserve (L_R,L_G,L_B). This class of techniques is called *backlight scaling*. Note that (t_R,t_G,t_B) are bounded by [0,1]. When (t_R,t_G,t_B) need to be greater than 1, the original luminance can not be recovered and image distortion in terms of brightness/contrast occurs.

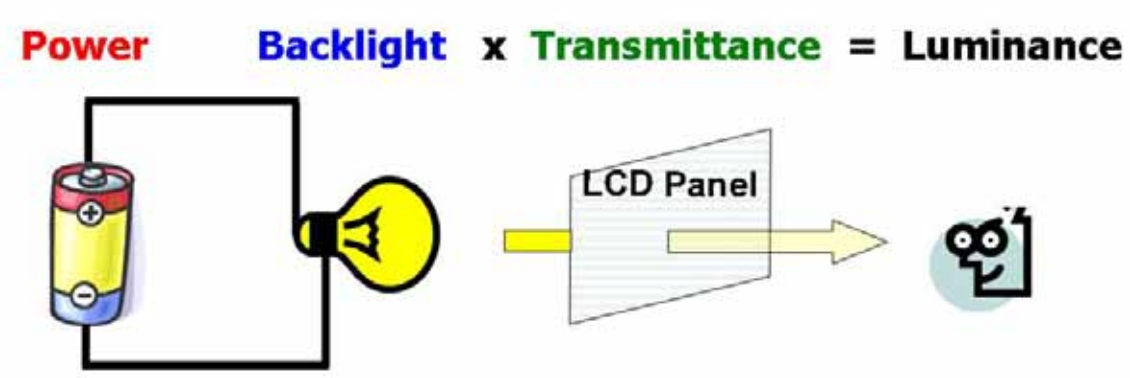

Figure 4-1: Backlight scaling concept: For minimizing the power consumption, the backlight scaling technique decreases the backlight duty cycle or intensity and increases the panel transmittance to keep the luminance.

4.3 Backlight Scaling Algorithms

Backlight scaling is by far the most effective technique for reducing power consumption in a transmissive display. To compensate for the visual quality loss due to reduced luminance,

proper image enhancement is necessary. Choi *et al.* proposed a technique that increases the pixel values (t) to recover the original luminance (L) [Choi 2004].

$$\begin{bmatrix} L_R \\ L_G \\ L_B \end{bmatrix} = (\alpha \cdot b_W) \cdot \begin{bmatrix} t_R / \alpha \\ t_G / \alpha \\ t_B / \alpha \end{bmatrix} \tag{14}$$

Choi's algorithm can preserve the luminance of the dark regions, but the bright regions will be over-saturated. In their study, the number of over-saturated pixels was chosen to evaluate the image quality loss.

Since preserving the original luminance is not always possible, finding a proper alternative transformation of luminance, $L^*=f(L)$, is the key of backlight scaling algorithms. Cheng *et al.* proposed an algorithm to compensate for the luminance loss by increasing the contrast [Cheng 2004]. The following linear transformation was used:

$$L^* = \begin{cases} 0, & L < gl \\ c(L - gl), & gl \le L \le gu \\ \alpha \cdot b_W, & gu < L \end{cases} \tag{15}$$

Where c, gl, and gu are constants generated by the optimization algorithm. Although Cheng's algorithm is a compromise between preserving the brightness and preserving the contrast, it does preserve the original tonality, i.e., the proportional difference between bright and dark regions. The relationship between brightness and contrast, however, was employed without substantial support.

Iranli *et al.* proposed using *histogram equalization*, an image processing algorithm that balances the number of pixels on each gray-level, to perform the image enhancement [Iranli 2005]:

$$L^* = h'(L), \tag{16}$$

Where h' is the derivative of the cumulative distribution function of the histogram.

Histogram equalization can reproduce each gray level distinctly without over-saturation or under-saturation. However, tonality will be distorted when the original histogram tends to be irregular.

(a) Original image		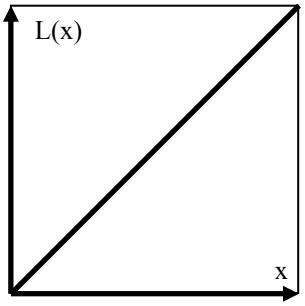
(b) Dim backlight to 50% without compensation for saving power	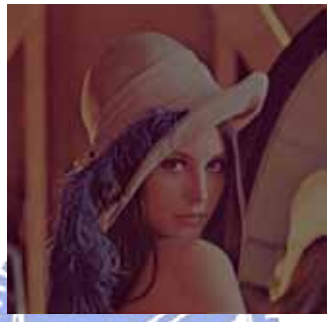	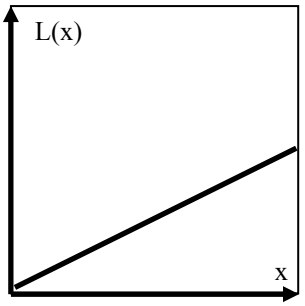
(c) Enhance contrast to recover brightness but pixels over-saturated	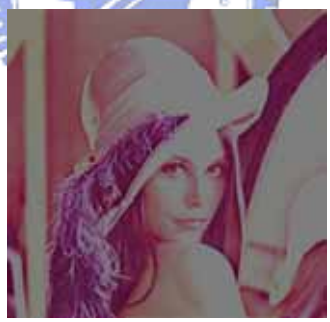	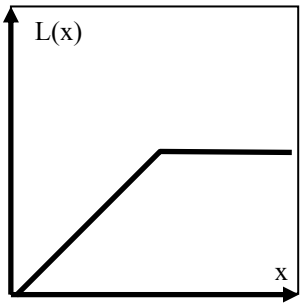
(d) Optimal CBCS based on histogram		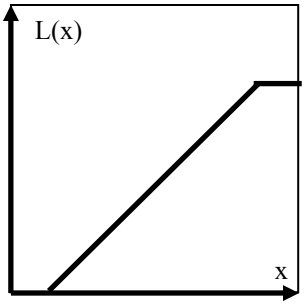

Figure 4-2: Concurrent Brightness and Contrast Scaling Concept.

4.4 Backlight Blinking

Conventional requirements of backlight design are spatial, temporal, and chromatic uniformity. Recently, the modern LCD technologies call for different backlight driving methods. For example, *backlight blinking* is adopted by LCD-TVs to deal with the *motion blur* problem. Unlike CRT monitors, because of the longer response time of liquid crystals, when steady backlight is used in an LCD, the fast moving edges appear to be blurred and degrade the sharpness of motion pictures. One solution is to pulse-drive (or "blink") the backlight in order to generate CRT-like pulses. According to temporal vision study, a pulse-type display (e.g. CRT) is immune from motion blur than a hold-type display (e.g. LCD).

For a blinking backlight driven by square wave of frequency f, duty cycle d, and intensity b_w, equation (17) can be rewritten as:

$$\begin{bmatrix} L_R \\ L_G \\ L_B \end{bmatrix} = (d \cdot b_W) \cdot \begin{bmatrix} t_R \\ t_G \\ t_B \end{bmatrix}. \tag{18}$$

The duration of each blink is d/f. Although the time-average luminance can be simply determined to be $d \cdot b_w$, the perceived brightness of blinking backlight, however, is not a simple function of luminance.

4.5 Brightness of Flashing Light

The *Talbot-Plateau* law states that the brightness of a temporally modulated stimulus, when fused, is equal to the brightness of a steady light with the same time-averaged luminance. The concept is similar to pulse-width-modulation (PWM). Consider a series of flashes in a square waveform, which can be qualified by its frequency f, duty cycle d, and intensity (magnitude) m. The Talbot-Plateau law recognizes that two flashing lights have the same brightness if $m_1 d_1 = m_2 d_2$. Note that when d=100% the light is steady. In other words, if two flashing lights have the same time-average luminance, they have the same brightness.

The *Broca-Sulzer effect* states that the supra-threshold stimuli, whose duration is on the order of 50-100 milliseconds, appear brighter than stimuli of either shorter or longer durations [Broca 1902]. This effect was discovered in 1902, when the flashing pattern of lighthouses was of great interest. The findings still inspire the design of electronics nowadays, for example, how to design the flashing pattern of the LED warning indicators of a cell phone such that it can efficiently draw the user's attention with minimum energy. Figure 2-1 depicts the time course of flashing lights of different intensity.

The *Broca-Sulzer effect* cannot be intuitively comprehended based on daily visual experience: A longer flash looks dimmer than a shorter flash. For example, "a 50ms light looks dimmer than a 40ms light" means that our visual sensation of a 40ms flash will be subtracted 10ms later. The phenomenon has been revisited by modern techniques and found to be caused by the neural mechanism.

The *Brücke brightness enhancement effect* is that when a light is flickered on and off, its brightness varies according to the frequency of flicker, reaching a maximum over a narrow range of frequencies at approximately 5 to 20 Hz, depending on the intensity of the flickering light [Moses 1987].

4.6 Flickering

The *critical flicker fusion frequency* (CFFF) indicates the transition from the perception of flicker to that of fusion occurs over a range of temporal frequencies. The *Ferry-Porter law* predicts that the CFFF increases as the luminance of the flashing stimulus increases:

$$f_{CFF}(L) = a \cdot \log(L) + b. \tag{19}$$

The CFFF is not only a function of luminance, but also the stimulus size (*Franit-Harper law*), wavelength (*Hecht-Shlaer law*), etc. In this paper, only luminance is considered, because the display size is fixed and the colors of displayed image have to be preserved.

4.7 Proposed Algorithm

The proposed algorithm presents a backlight driving technique that concurrently saves power and maintains perceived brightness for liquid crystal displays by scaling the intensity, frequency, and duty cycle of its LED backlights. The algorithm applies the *Brücke brightness enhancement effect* to compensate the perceived brightness loss while the backlight is modulated temporally.

To give an example, the luminance of a blinking backlight with 50% duty cycle decreases half of luminance. For compensating the loss of luminance, the backlight intensity must be increased by LED driver but that can not save power. For saving power and keeping perceived brightness simultaneously, a new backlight driving method is to decrease frequency without increasing intensity or duty cycle. The human eye can feel brighter when backlight blinking frequency under CFFF so that the same perceived brightness only consumes half of power because of 50% duty cycle and the same intensity.

One requirement for such algorithms is to have a model of perceived brightness enhancement. This model can report to the algorithm observer perceived brightness based on the modulated frequency. Then the power savings can be estimated while the relation between luminance and power consumption is characterized. In chapters, some measurements and psychophysical experiments will be done for verifying the proposed algorithm.

4.8 Summary

Compared with the previous backlight scaling algorithms, the proposed backlight driving scheme can save power and keep perceived brightness independent of the image content. The amount of brightness enhancement can be estimated from the experimental results. In the following chapter, the psychophysical experiments will be done.

Chapter 5

Experimental results and Evaluation

We conducted visual experiments to parameterize the Brücke brightness enhancement effect, Ferry-Porter law and the relationship between favorite display luminance and ambient light.

5.1 Apparatus

To demonstrate our concept, we measured and characterized the power and energy consumption of an Apple iPod®, which is capable of playing MP3 music and MPEG4-compressed video clips. Its major components include a hard-disk, a LED-backlit LCD, a lithium-ion battery, a button/wheel interface, and a video processor, as shown in Figure 5-1.

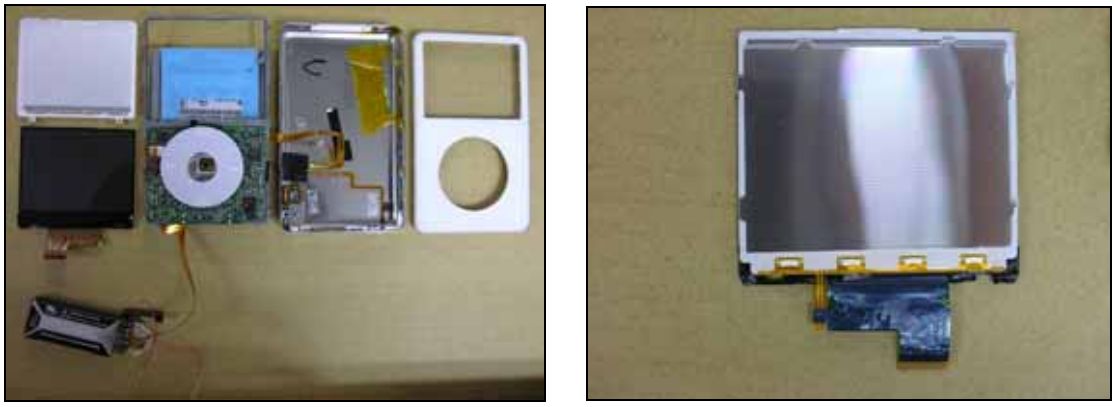

Figure 5-1: iPod's backlight consists of four white LEDs in series.

Figure 5-2 shows the power profile of playing a video clip. The spikes in the very beginning occurred when a video clip started to play. The hard disk drive consumed a significant amount of power. The following table lists the power consumed in different states of the 1.8" dual-disk 4,200 rpm hard disk drive Toshiba MK6008GAH.

State	Power (mW)
Start	1800
Reading, Writing, Seeking	1000 - 1100
Idle	400
Standby, Sleep	7 - 12

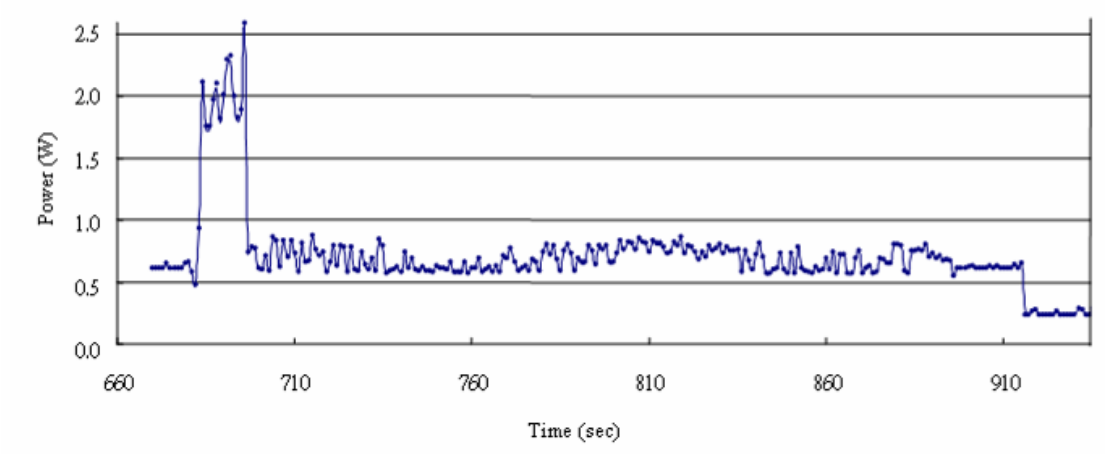

Figure 5-2: Power profiling of iPod playing a 323-second video clip.

5.2 Instruments

The luminance and chromaticity coordinates of stimuli are the key properties of system for calibration and evaluation. In order to obtain this information, a colorimeter is necessary. We chose the Konika-Minolta Chroma Meter CS-200, which utilizes three high-sensitivity silicon photo cells, which were filtered to match the *Commission International de I'Eclairage* (CIE) standard observer response. Chromaticity coordinates (x,y) and luminance (L) as well as color temperature in Kelvin (K) were calculated from the three cells' measurements. With this compact reliable color analyzer, the luminance and chromaticity coordinates of stimuli were obtained [Minolta].

The frequency and duty cycle of temporal modulated stimuli were controlled by the function generator (Agilent Technologies 33220A), a 20 MHz synthesized function generator

with built-in arbitrary waveform and pulse capabilities. The Agilent 33220A can generate frequency from 10^{-6} to 2×10^{7} Hz with 10^{-6} Hz resolution. The standard waveforms (such as sine or square wave) and arbitrary waveforms can be generated or intermittently. Those arbitrary waveforms can be created by the software, Agilent IntuiLink, using graphic user interface on the PC, and then downloaded into the Agilent 33220A through USB cable. With Agilent 33220A, we can generate arbitrary frequency and duty cycle of temporal modulated stimuli for the LED backlight [Agilent].

The DC power supply, Good Will Instrument PPT-3615G, supplies constant direct current to the LEDs. It has three programmable channels that two of them have adjustable voltage from 0 to 36V as well as adjustable current from 0 to 1.5A. The other has adjustable voltage from 0 to 6V and adjustable current from 0 to 3A [GoodWill b]. Due to the restrictions of PPT-3615G, the serial voltage of LEDs in one series can not exceed 36V as well as the parallel current of LEDs which summed up each series can not exceed 3A.

The power consumption can be calculated by the current and voltage that were measured by digital multimeters. For measuring both the current and voltage simultaneously, two multimeters were needed to measure each power line. For this purpose, the multimeter Good Will Instrument GDM-8246 was chosen [GoodWill a].

(a)

(b)

(c) (d)

Figure 5-3: The instruments: (a) Konika-Minota Chroma Meter CS-200, (b) Agilent Technology 33220A, (c) Good Will Instrument PPT-3615G, and (d) Good Will Instrument GDM-8246.

5.3 Luminance and Power Modeling

In Figure 5-4, the power supply supplied the constant voltage and adjustable current to the LED backlight. The voltage was read from the power supply and the current was read from the multi-meter simultaneously. In the meantime, the luminance of LCD panel was measured by the CS-200.

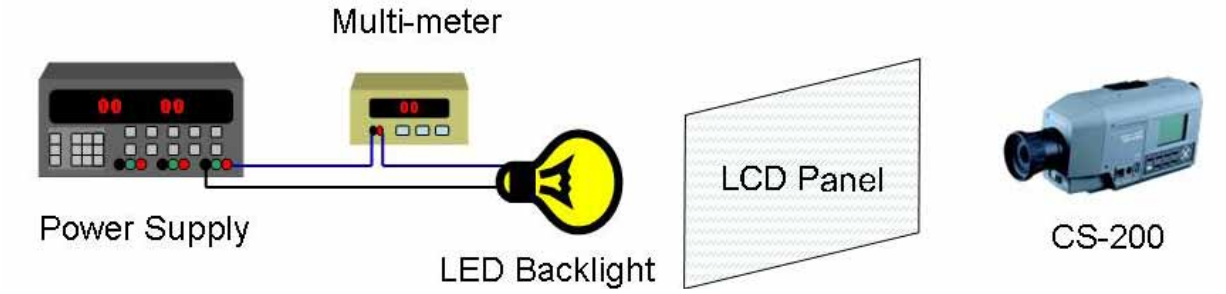

Figure 5-4: The experimental environment setup for luminance and power modeling.

For measuring thirteen samples of luminance and power data, the current was adjusted from 2 to 26 mA with 2 mA increment. For each sample, the voltage and the luminance were recorded at the same time. The power consumption was calculated by multiplying current and voltage and the results are shown in Figure 5-5.

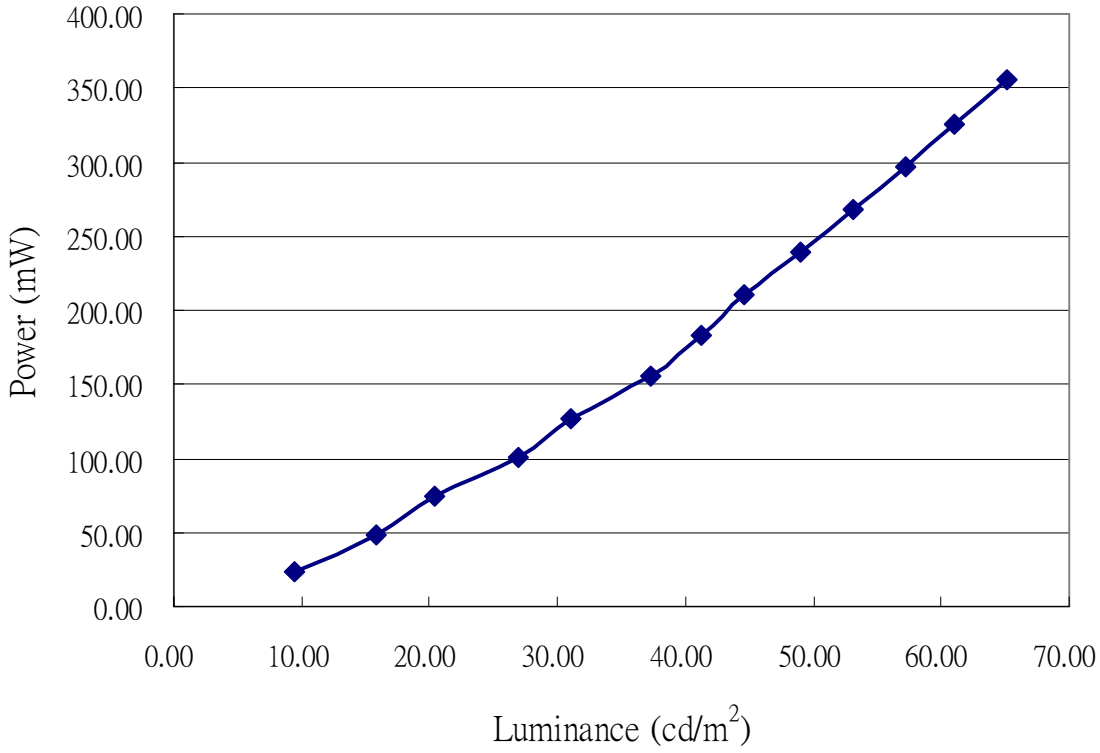

Figure 5-5: Power vs. luminance of the iPod backlight.

Based on the measurement data, the luminance vs. power relationship can be modeled by the following quadratic function:

$$P = 0.0374b^2 + 3.2194b - 10.5760 \quad \text{(mW)} \tag{20}$$

Where b is backlight luminance.

5.4 Perceptual Flicker Modeling

The conventional psychophysical *method of adjustment* was used to find the CFFF of three observers in a dark room [Sekuler 1994]. We designed a pair of LED lights for this experiment. The 4cm*5.5cm light was placed 70 cm away from the observer. The light was driven by 50% square waveforms at frequency 20, 25, 30, 35, and 40 Hz. The experimental conditions are illustrated in Figure 5-6.

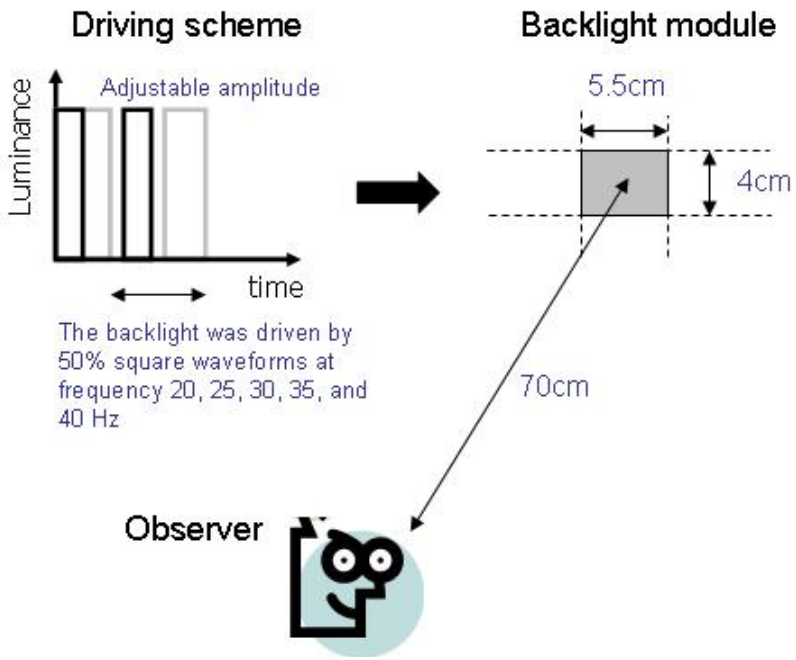

Figure 5-6: The experimental environment for perceptual flicker modeling.

Each observer was asked to find the CFFF by adjusting the luminance. The results are shown in Figure 5-7. Figure 5-8 was obtained by redrawing Figure 5-7 after replacing the y-axis/x-axis with logarithmic luminance.

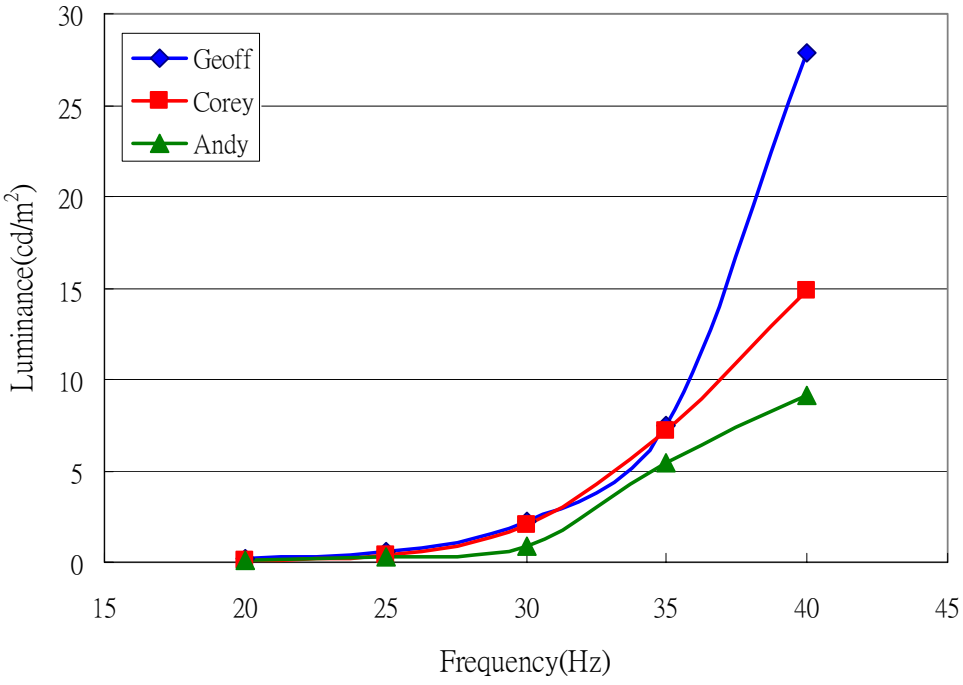

Figure 5-7: Experimental data of the perceptional flicker modeling from three observers.

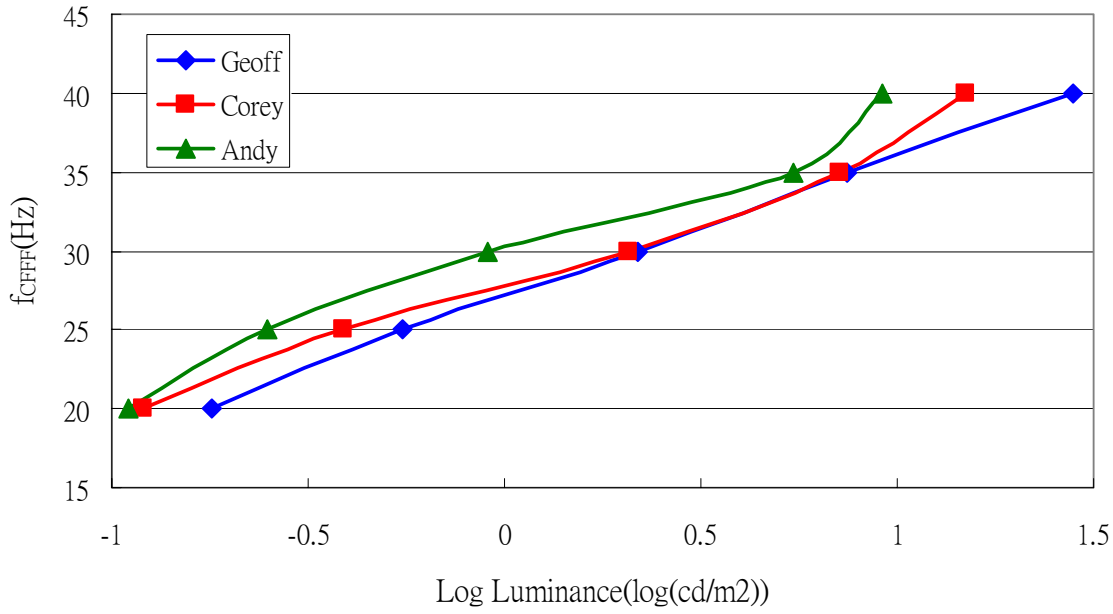

Figure 5-8: Experimental data of the perceptional flicker modeling from three observers as f_{CFFF} vs. log(luminance).

By linearly fitting the data to equation (21), the perceived flicker can be modeled as

$$f_{CFFF}(L) = 9\log(L) + 28. \tag{22}$$

5.5 Brightness Enhancement Modeling

The brightness enhancement effect was demonstrated by having an observer compare the brightness of two flashes: a test flash and a control flash. The test flash was of variable duration and constant intensity. The control flash was of constant duration and variable intensity. The observer's task was to adjust the intensity of the control flash such that it matched the brightness of the test flash. Over the course of an experiment, the test flash was presented in a large number of durations, and for each of the durations, the observer adjusted the intensity of the control flash so that it matched the brightness of the test flash. The experimental setup is described in Figure 5-9.

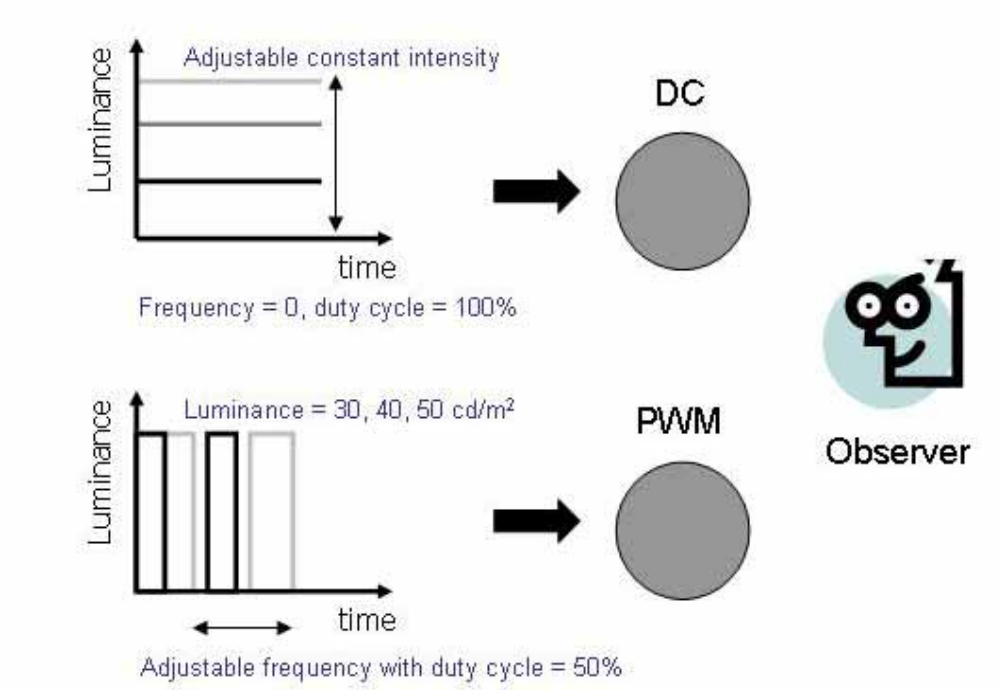

Figure 5-9: Experimental setup for the brightness enhancement effect: An observer saw two circle stimuli simultaneous and adjusted the flashing duration of test light to match the brightness of control light for each variable luminance.

In the experiment of Brücke effect, two 1-degree white LED lights were placed side by side for the observer to match. One was driven by adjustable constant intensity, while the other was driven by 50% square waveforms over a range of 30, 40, and 50 cd/m^2. Each observer was asked to match the brightness by adjusting the steady light. The results are shown in Figure 5-10.

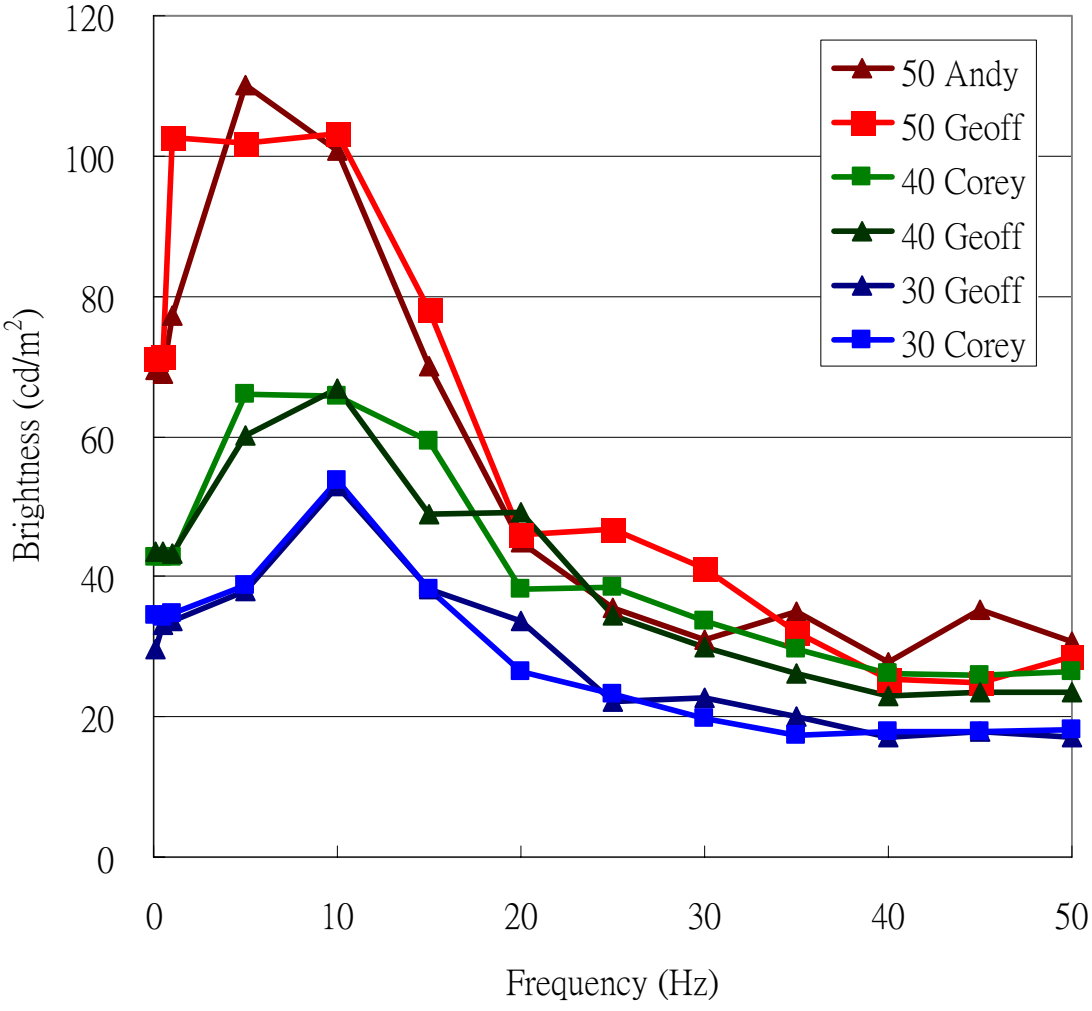

Figure 5-10: Experimental data of the brightness enhancement effect: brightness vs. frequency from 3 observers at luminance 30, 40, and 50 cd/m^2.

In Figure 5-10, flashes with higher intensity have higher brightness. According to equation (9), the CFFFs are 43, 42, and 41 Hz for 50, 40, and 30 cd/m^2, respectively. Beyond 43 Hz, the brightness was about half of the intensity because of the 50% duty cycle. When the frequency approached to zero (DC), the brightness reached about the full intensity. At these low frequencies, the observers could distinct the on-cycles from the off-cycles and chose the high brightness of on-cycles to match. The brightness reached the maximum of about twice intensity around 10 Hz. The frequency range between CFFF and 10 Hz of Figure 5-10 is redrawn as brightness vs. period in Figure 5-11.

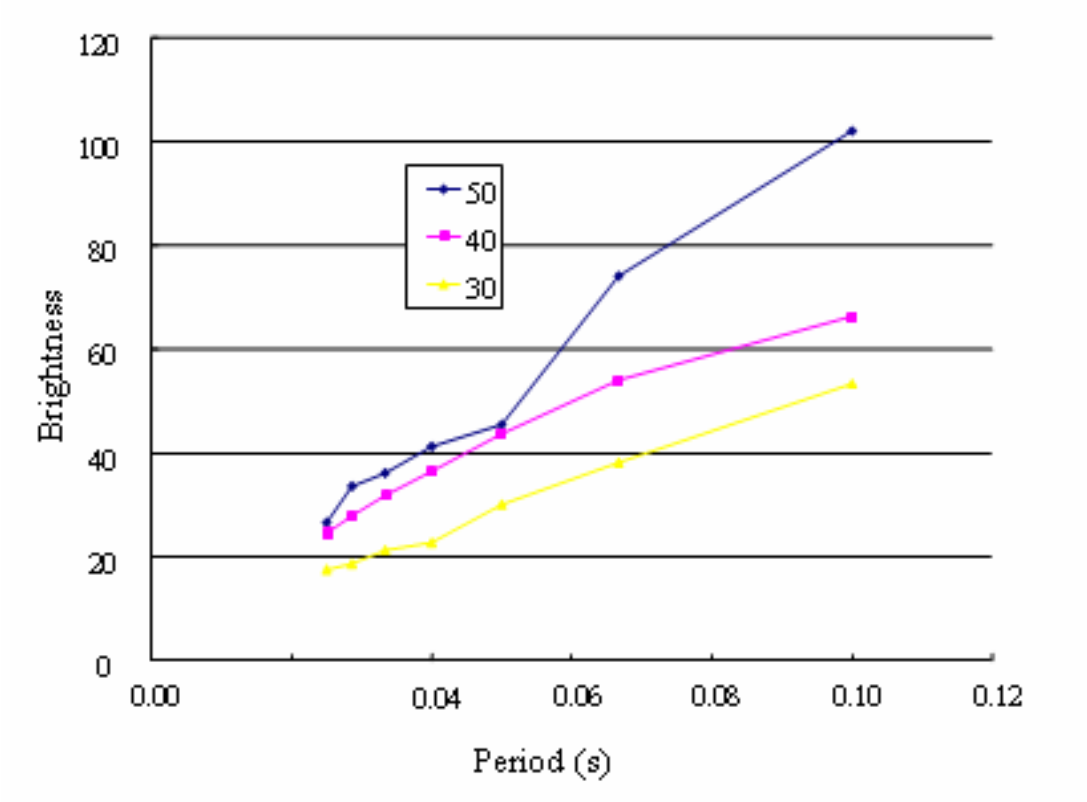

Figure 5-11: In the range between CFFF (≅ 42 Hz) and 10 Hz, the relationship between brightness and 1/*f* can be linearly approximated.

Summarizing the above observations, we can approximate the Brücke effect by:

$$L'_{50\%}(L,f) = \begin{cases} L/2, & f_{CFF}(L) < f \\ \frac{L}{2} + \left(\frac{1}{f} - \frac{1}{f_{CFF}(L)}\right)\left(\frac{3L/2}{0.1 - \frac{1}{f_{CFF}(L)}}\right), & 10 < f < f_{CFF}(L). \end{cases} \quad (23)$$

5.6 Surrounding Effects

The surround luminance is one of the most important factors in visual sensation. When the user adapts to a dark surround, he/she may dim the backlight to the lowest level and still has the full range of lightness and chroma. In the mean time, a considerable amount of power savings is achieved without any side effect. In literature of display ergonomics such as TCO'03, the luminance ratio of display to surround is recommended to be set between 10:1 and 100:1 [TCO03]. We conducted visual experiments to find the relationship between

favorite display luminance vs. surround luminance. We visited three users in different offices and measured the surround illuminance. The users were asked to perform different tasks at different levels of surround illuminance with their favorite display luminance. If we assume the reflectance of the surround is similar to middle gray (i.e. 18% reflectance, Munsell N5), then the reflected luminance can be estimated as a linear function of illuminance. The results are shown in Figure 5-12.

The tasks included movie watching, web surfing, and text editing. Generally the favorite display luminance increases linearly as the surround illuminance. The movie watching task had much lower display luminance because the display was driven in the *direct draw* mode. For the same user, text editing had lower display luminance than web surfing in order to reduce eye strain. The curves have different trends in the bright portion (>100 lux) and dark portion (<100 lux). The reason may be the users switching between the photopic mode (light adapted, cone-dominating) and scotopic mode (dark adapted, rod-dominating).

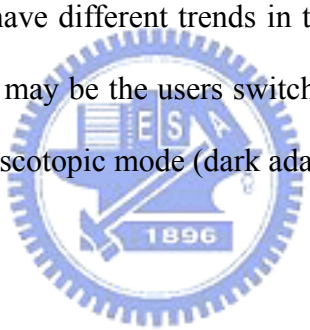

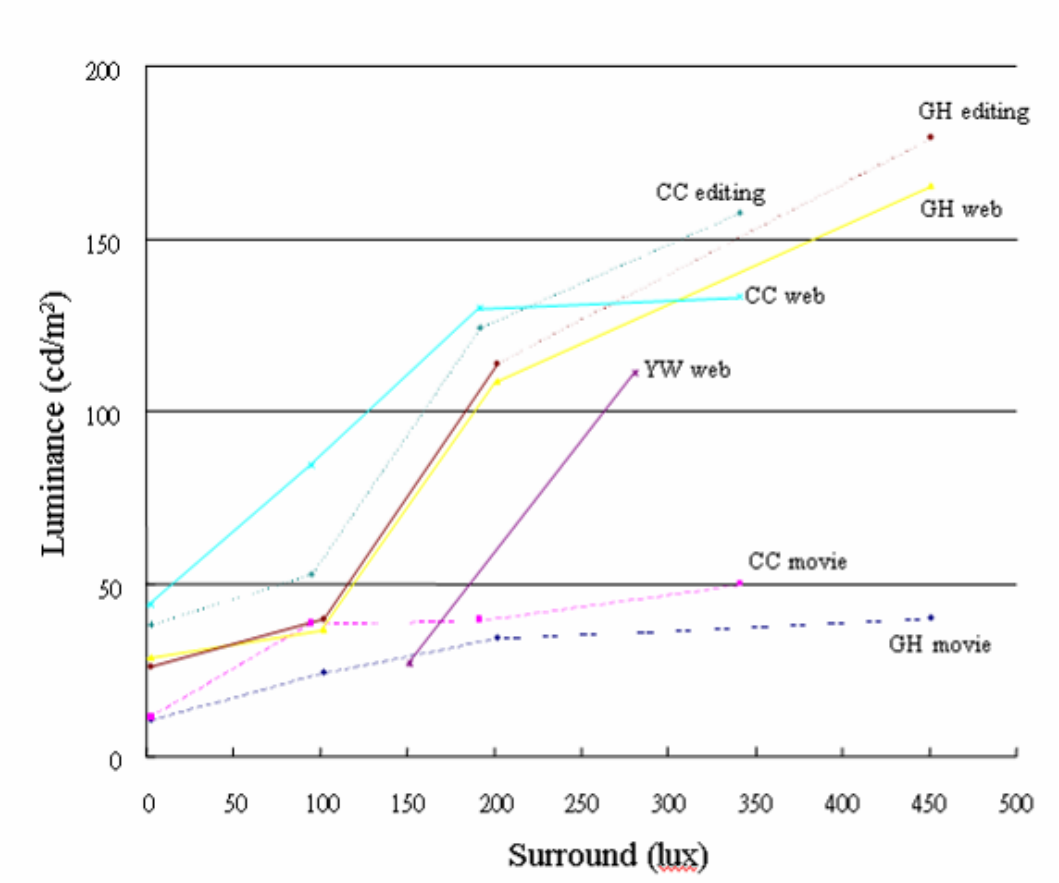

Figure 5-12: Favorite display luminance vs. surround illuminance of three users on movie watching, web surfing, and text editing.

5.7 Evaluation

For evaluating the proposed algorithm, the prototype consists the four blocks as shown in Figure 5-13. In the head of the system block, the photo-sensor module detects the ambient light and provided the FPGA module the ambient light levels. Next, the FPGA module determined what kind of environments was located due to the information of ambient light levels. The LED driver drove the LED backlight module by the driving scheme that was provided from the FPGA module. The backlight emitted the light depending on the proposed algorithm implemented in the FPGA module.

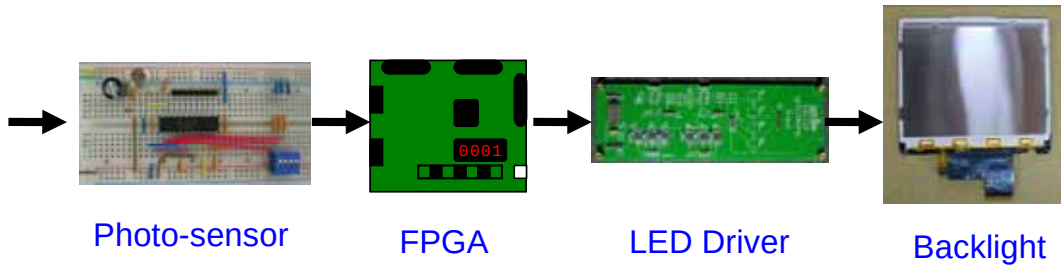

Figure 5-13: The system block diagram consisted a photo-sensor module, FPGA module, LED driver, and LED backlight module.

For the brightness of a steady light of luminance L, we blinked the backlight with the following duty cycle, magnitude and frequency instead:

$$d^* = 50\% \tag{24}$$

$$m^* = L/2 \tag{25}$$

$$f^* = \frac{2}{3} f_{CFF}(L) + \frac{10}{3}. \tag{26}$$

Based on equation (23), the magnitude and frequency of the backlight could be reduced while keeping the same brightness. The power consumption was estimated as listed in Table 5-1. In the last two columns, R_L represents the brightness ratio of $L'_{50\%}$ to L ($R_L = L'_{50\%}/L$) and R_P represents the power consumption ratio of $P_{L'50\%}$ to P_L ($R_P = P_{L'50\%}/P_{L)}$ while $L'_{50\%}$ is perceived brightness at f* with 50% duty cycle.

Table 5-1: The brightness enhancement ratio and power consumption ratio were listed by different driving frequency:

L (nit)	P_L(mW)	f_{CFFF} (Hz)	f* (Hz)	$L'_{50\%}$ (nit)	$P_{L'50\%}$ (mW)	R_L	R_P
32.5	133.6	41.6	40.0	33.1	137.1	102%	97%
32.5	133.6	41.6	35.0	35.4	150.3	109%	89%
32.5	133.6	41.6	30.0	38.5	168.6	118%	79%
32.5	133.6	41.6	25.0	42.7	195.4	132%	68%

32.5	133.6	41.6	20.0	49.2	238.1	151%	56%
32.5	133.6	41.6	15.0	59.9	316.1	184%	42%
32.5	133.6	41.6	10.0	81.3	497.9	250%	27%

When the baseline backlight power is 100%, the proposed technique can decrease power consumption to 68% while preserving the same brightness at the cost of flickering. When the baseline backlight brightness was 100%, the proposed technique can increase the brightness up to 132% while keeping the same power consumption at the cost of flickering. The power saving ratio decreases and the brightness enhancement increases with decreased f*. However, the increase of brightness enhancement becomes less due to Broca-Sulzer effect, which has a peak of brightness enhancement at 50ms duration as well as 10 Hz with 50% duty cycle.

The visual effects of different techniques were shown as Figure 5-14. In Figure 5-14 (a), higher gray level pixels are over saturated when Choi's algorithm was used. In Figure 5-14 (b), the tone of image was changed when Iranli's algorithm was used. In Figure 5-14 (c) when Cheng's algorithm was used, both higher and lower gray level pixels was cut but better than (a). In the figure (a), (b), or (c), more power savings lead to more distortion. However, applying the proposed algorithm did not cause spatial distortion but flickering in the temporal domain.

(a)

(b)

(c) **(d)**

Figure 5-14: Simulated visual effects of (a) Choi, (b) Iranli, (c) Cheng, and (d) the proposed algorithm without showing the flickering.

5.8 Summary

The psychophysical experiments had been performed and the relationship between perceived brightness and modulated light frequency had been modeled based on its results. By using this model, the power savings can be estimated. The proposed algorithm can reduce power consumption down to 68% while preserving the same brightness or can increase brightness up to 132% at the cost of flickering.

Chapter 6

Conclusions and Future Direction

6.1 Conclusions

The temporal properties of human vision system such as Broca-Sulzer effect and Brücke-Bartley effect have been reviewed and applied to the low-power LCD. For modeling the relationship between perceived brightness and modulated light frequency, psychophysical experiments have been performed. According to the experimental results, a novel backlight driving technique for liquid crystal displays has been presented. By scaling the intensity, frequency, and duty cycle of the backlight, this technique not only increases the perceived brightness but also prolongs the service time of rechargeable batteries. A great amount of energy can be saved at the cost of flickering. The Brücke brightness enhancement effect from temporal properties of vision system was employed in customizing LED backlight modules.

6.2 Future Direction

Although the preliminary results are encouraging, this study is still in its infancy. Hence, the future direction may extend the temporal domain to the spatial domain through spatial-temporal contrast sensitivity surface and include developing a metric for measuring the flickering, refining the visual experiments, and FPGA implementation. Furthermore, the brightness enhancement of temporal properties of vision is applicable to the emergency light or traffic light.

References

[Agilent] Agilent Technology, 33220A Function Generator.

[Anandan 2006] M. Anandan, ”LED Backlight for LCD/TV Monitor: Issues that Remain”, SID06’ DIGEST, pp. 1509-1512, 2006.

[Anstis 1983] S. M. Anstis and P. Cavanagh, “A minimum motion technique for judging equiluminance,” in Color Vision: Physiology and Psychophysics, J. D. Mollon and L. T. Sharpe, eds., pp. 155-166, 1983.

[Arend 1994] L. Arend, J. Lubin, J. Gille, J. Larimer, “Color breakup in sequentially scanned LCDs,” SID 94 Digest, pp. 201-204, 1994.

[Arima] Arima Optoelectronics Corporation, 7F, No.349, Sec. 2, Renhe Rd., Dashi, Taoyuan 335, Taiwan (R.O.C.), 5W RGGB LED Emitter.

[Broca 1902] A. Broca, D. Sulzer, “La sensation lumineuse en fonction du temps,” Academie Des Sciences, pp. 831-835, 1902.

[Cheng 2004] W-C. Cheng and M. Pedram, “Power minimization in a backlit TFT-LCD display by concurrent brightness and contrast scaling,” Proc. of Design Automation and Test in Europe, pp. 252-259, 2004.

[Cheng 2006] W-C. Cheng, C-F. Hsu, and C-F. Chao, "Temporal vision-guided energy minimization for portable displays," Proc. of International Symposium on Low Power Electronics and Design, pp.89-94, 2006.

[Choi 2004] N. Chang, I. Choi, H. Shim, “DLS: Dynamic backlight luminance scaling of liquid crystal display,” IEEE Tran. VLSI, Vol. 12, No. 8, pp. 837-846, 2004.

[ConoScope] http://www.autronic-melchers.com/

[Farrell 1987] J. E. Farrell, B. L. Benson, C. R. Haynie, “Predicting flicker thresholds for video display terminals,” Proceedings of the SID, Vol. 28, pp. 449-453, 1987.

[GoodWill a] Good Will Instrument Co., Ltd., No. 7-1, Jhongsing Rd., Tucheng, Taipei, 236, Taiwan (R.O.C.), GDM-8246 multi-meter.

[GoodWill b] Good Will Instrument Co., Ltd., No. 7-1, Jhongsing Rd., Tucheng, Taipei, 236, Taiwan (R.O.C.), PPS-3635G Programmable DC power supply.

[Hecht 1933] S. Hecht, and C. D. Verrijp, “Intermittent stimulation by light. III. The relation between intensity and critical fusion frequency for different retinal locations,” J. Gen. Physiol., Vol. 17, pp. 251-268, 1933.

[Huang 2000] H. C. Huang, P. W. Cheng, and H. S. Kwok, “On the Minimization of Flicker and Image Retention in Silicon Light Valves,” SID 00 Digest, pp. 248-251, 2000.

[Hunt 1995] R. W. G. Hunt, *Measuring Colour, 3rd Ed.*, Fountain Press, England, 1998

[Iranli 2005] A. Iranli, H. Fatemi, and M. Pedram, “HEBS: Histogram equalization for backlight scaling,” Proc. of Design Automation and Test in Europe, pp. 346-351, 2005.

[Kelly 1961] D. H. Kelly, “Visual responses to time-dependent stimuli. I. Amplitude sensitivity measurements,” J. Opt. Soc. Am., Vol. 51, pp. 422-429, 1961.
[Kelly 1966] D. H. Kelly, “Frequency doubling in visual responses,” J. Opt. Soc. Am., Vol. 56, pp. 1628-1633, 1966.
[Kelly 1972] D. H. Kelly, “Adaptation effects on spatio-temporal sine-wave thresholds,” Vision Res., Vol. 12, pp. 89-101, 1972
[Kelly 1974] D. H. Kelly, “Spatio-temporal frequency characteristics of color-vision mechanisms,” J. Opt. Soc. Am., Vol. 64, pp. 983-990, 1974.
[Kelly 1977] D. H. Kelly, D. van Norren, “Two-band model of heterochromatic flicker,” J. Opt. Soc. Am., Vol. 67, pp. 1081-1091, 1977.
[Kelly 1979] D. H. Kelly, “Motion and vision. II. Stabilized spatio-temporal threshold surface,” J. Opt. Soc. Am., Vol. 69, No. 10, pp. 1340-1349, 1979.
[Kelly 1981] D. H. Kelly, “Disappearance of stabilized chromatic gratings,” Science, Vol. 214, pp. 1257-1258, 1981.
[Kelly 1983] D. H. Kelly, “Spatiotemporal variation of chromatic and achromatic contrast thresholds,” J. Opt. Soc. Am., Vol. 73, No. 6, pp. 742-750, 1983.
[Kelly 1994] D. H. Kelly, *Visual Science and Engineering*, Marcel Dekker, 1994.
[Koma 2000] N. Koma, T. Miyashita, T. Uchida, and N. Mitani, “Color field sequential LCD using an OCB-TFT-LCD,” SID 00 Digest, pp. 632-635, 2000.
[Laird 2006] J. Laird, M. Rosen, J. Pelz, E. Montag, and S. Daly, “Spatio-velocity CSF as a function of retinal velocity using unstabilized stimuli,” Proc. of SPIE-IS&T Electronic Imaging, Vol. 6057, 605705, 2006.
[Lee 2005] S. H. Lee, S. W. Jang, E. S. Kim, S. H. Lee, and K. I. Sohng, “The design of an LCD system based on the quantitative analysis for enhancement of the motion picture quality,” IEICE Trans. ELECTRON., Vol. E88-C, No. 11, pp. 2094-2098, 2005.
[Lee 2006] J. W. Lee et al., “Amorphous silicon based 40” LCD TV using ultra fast OCB mode,” SID 06 Digest, pp. 1950-1953, 2006.
[Liu 2005] J. Liu, B. A. Wandell, “Specializations for chromatic and temporal signals in human visual cortex,” Journal of Neuroscience, Vol. 25, pp. 3459-3468, 2005.
[Minolta] Konika-Minolta, Chroma Meter CS-200.
[Moses 1987] R. A. Moses, and W. M. Hart, Jr., *Adler’s Physiology of the Eye, 8th Ed.*, Washington, DC: The C. B. Mosby Company, 1987.
[Post 1997] D. L. Post, P. Monnier, and C. S. Calhoun, “Predicting color breakup on field-sequential displays,” Proceedings of SPIE: Head-Mounted Displays II, 3058, pp. 57-65, 1997.
[Salters 2001] B. Salters, R. van Dijk, “Reduction of large area flicker in plasma display panels,” SID 01 Digest, pp. 1098-1101, 2001.
[Schwartz 1994] S. H. Schwartz, *Visual Perception: A Clinical Orientation*, Appleton & Lange, 1994.

[Sekuler 1994] R. Sekuler and R. Blake, *Perception, 3rd Ed.*, NY: McGraw-Hill, 1994.
[Silverstein 2005] L. D. Silverstein, "STColor: Hybrid spatial-temporal color synthesis for enhanced display image quality," SID 05 Digest, pp. 1112-1115, 2005.
[SiTI] SiTI, No. 9-7F-1, Prosperity Rd. I, Science-Based Industrial Park, Hsinchu, 300, Taiwan (R.O.C.), DD311 High Constant Current LED Driver.
[Sun 2006] P. L. Sun, "A simple approach to reduce color breakup for field-sequential color LCDs," Taiwan Display Conference 2006, pp. 314-317, 2006.
[Swanson 1987] W. H. Swanson, T. Ueno, V. C. Smith, and J. Pokorny, "Temporal modulation sensitivity and pulse-detection thresholds for chromatic and luminance perturbations," J. Opt. Soc. Am. A, Vol. 4, pp. 1992-2005, 1987.
[TCO03] http://www.tcodevelopment.com/
[Uchida 2006] T. Uchida et al., "Color imaging and display system with field sequential OCB LCD," SID 06 Digest, pp. 116-169, 2006.
[Varner 1984] D. Varner, "Temporal sensitivities related to color theory," J. Opt. Soc. Am. A, Vol. 1, pp. 474-481, 1984.
[ViewSonic] ViewSonic, No. 381, Brea Canyon Rd., Walnut, California, 91789, USA, VX912 LCD Monitor.
[Wagner 1972] G. Wagner, and R. M. Boynton, "Comparison of four methods of heterochromatic photometry," J. Opt. Soc. Am., Vol. 62, pp. 1508-1515, 1972.
[Wandell 1995] B. A. Wandell, *Foundations of Vision*, Sinauer Associates, 1995.
[Wyszecki 1982] G. Wyszecki, W. S. Stiles, *Color Science, 2nd Ed.*, John Wiley and Sons, 1982.
[Yamagishi 2006] N. Yamagishi, Y. Tanabe, H. Ishibashi, and H. Yamagami, "Moving picture simulations with OCB for image-blurring-free LC TVs," SID 06 Digest, pp. 1804-1807, 2006.
[YEH 1999] P. Yeh, and C. Gu, *Optics of Liquid Crystal Displays*, John Wiley & Sons, New York, 1999.
[Zwanenburg 2004] M. J. Zwanenburg et al., "High-efficiency LEDs for LCD backlights," SID 04 Digest, pp. 1222-1225, 2004.

Vita

A. GENERAL INFORMATION

Name: CHIH-FU Geoff HSU / 許枝福

E-mail: cfhsu.iod93g@nctu.edu.tw

B. EDUCATION

03/2005 - 02/2007	M.S. in Photonics and Display Technologies, National Chiao Tung University, Hsinchu, Taiwan Advisor: Dr. Wei-Chung Cheng
09/1998 - 06/2000	B.S. in Electronic Engineering National Taipei University of Technology, Taipei, Taiwan
09/1993 - 06/1998	Diploma in Electronic Engineering National Taipei Institute of Technology, Taipei, Taiwan

C. EXPERIENCE

09/2004 - 02/2005	Deputy Manager, Electrical Engineering Group, Multimedia Communications Division, TATUNG CO.
09/2002 - 08/2004	Engineer, Electrical Engineering Group, Multimedia Communications Division, TATUNG CO.
08/2000 - 08/2002	Enlistment at the Fourth Peace preservation Police Corps of the National Police Administrator

D. AWARD

- ✧ Best Paper Award, International Symposium on Low Power Electronics and Design 2006
- ✧ 96 年度教育部與經濟部產業研發碩士班聯合畢業典禮暨成果發表會優選獎

E. PUBLICATION

- ✧ C-F. Hsu and W-C. Cheng, "Theoretic Bounds on Panel Size of Flicker-free Field Sequential LCDs," *Asia Display 2007.*
- ✧ C-F. Hsu and W-C. Cheng, "Power Minimization for LCDs by Backlight Blinking," *Taiwan Display Conference 2006*, pp. 359-361.
- ✧ W-C. Cheng, C-F. Hsu, and C-F. Chao, "Temporal vision-guided energy minimization for portable displays," *Proc. of International Symposium on Low Power Electronics and Design 2006*, pp.89-94.